



Spin Change of Asteroid 2012 TC4 Probably by Radiation Torques

Hee-Jae Lee^{1,2} , Josef Āurech³ , David Vokrouhlický³ , Petr Pravec⁴, Hong-Kyu Moon², William Ryan⁵, Myung-Jin Kim², Chun-Hwey Kim¹ , Young-Jun Choi^{2,6}, Paolo Bacci⁷, Joe Pollock⁸, and Rolf Apitzsch⁹

¹ Chungbuk National University, 1 Chungdae-ro, Seowon-gu, Cheongju, Chungbuk 28644, Republic of Korea; hjlee@kasi.re.kr

² Korea Astronomy and Space Science Institute, 776, Daedeokdae-ro, Yuseong-gu, Daejeon 34055, Republic of Korea

³ Astronomical Institute, Faculty of Mathematics and Physics, Charles University, V Holešovičkách 2, 180 00 Prague 8, Czech Republic

⁴ Astronomical Institute, Academy of Sciences of the Czech Republic, Fričova 1, 251 65 Ondřejov, Czech Republic

⁵ New Mexico Institute of Mining and Technology, Socorro, NM 87801, USA

⁶ University of Science and Technology, 217, Gajeong-ro, Yuseong-gu, Daejeon 34113, Republic of Korea

⁷ Gruppo Astrofili Montagna Pistoiese, 51028 San Marcello Piteglio, Province of Pistoia, Italy

⁸ Physics and Astronomy Department, Appalachian State University, Boone, NC 28608, USA

⁹ Wildberg Observatory, D-72218 Wildberg, Germany

Received 2020 November 25; revised 2020 December 13; accepted 2020 December 16; published 2021 February 11

Abstract

Asteroid 2012 TC4 is a small (~ 10 m) near-Earth object that was observed during its Earth close approaches in 2012 and 2017. Earlier analyses of light curves revealed its excited rotation state. We collected all available photometric data from the two apparitions to reconstruct its rotation state and convex shape model. We show that light curves from 2012 and 2017 cannot be fitted with a single set of model parameters; the rotation and precession periods are significantly different for these two data sets, and they must have changed between or during the two apparitions. Nevertheless, we could fit all light curves with a dynamically self-consistent model assuming that the spin states of 2012 TC4 in 2012 and 2017 were different. To interpret our results, we developed a numerical model of its spin evolution in which we included two potentially relevant perturbations: (i) gravitational torque due to the Sun and Earth and (ii) radiation torque, known as the Yarkovsky–O’Keefe–Radzievskii–Paddack (YORP) effect. Despite our model simplicity, we found that the role of gravitational torques is negligible. Instead, we argue that the observed change of its spin state may be plausibly explained as a result of the YORP torque. To strengthen this interpretation, we verify that (i) the internal energy dissipation due to material inelasticity and (ii) an impact with a sufficiently large interplanetary particle are both highly unlikely causes of its observed spin state change. If true, this is the first case where the YORP effect has been detected for a tumbling body.

Unified Astronomy Thesaurus concepts: Asteroids (72); Close encounters (255); Near-Earth objects (1092); Small solar system bodies (1469)

Supporting material: data behind figures

1. Introduction

Apollo-type near-Earth asteroid 2012 TC4 was discovered in 2012 October by the Pan-STARRS1 survey, a few days before its closest approach to Earth (having a geocentric distance of about 95,000 km). It was observed photometrically, and its rotation period of about 12 minutes (Odden et al. 2013; Polishook 2013; Warner 2013; Carbognani 2014) and effective diameter of 7–34 m (Polishook 2013) were determined. Later, Ryan & Ryan (2017) noticed a second period in the data and interpreted it as a manifestation of a tumbling rotation state.

The next close approach in 2017 October was at a geocentric distance of about 50,000 km, and an even more extensive observing campaign (including spectroscopic and radar observations) was coordinated by the NASA Planetary Defense Coordination Office (PDCO) at that time. This campaign also served as a planetary defense exercise, and its results were summarized by Reddy et al. (2019). Additionally, Urakawa et al. (2019) also conducted the observing campaign of this asteroid in the same apparition independently and attempted to reproduce their light curves with a model of a tumbling triaxial ellipsoid. Besides these observing campaigns, a few photometric observations of 2012 TC4 were carried out in this apparition (Sonka et al. 2017; Warner 2018; Lin et al. 2019). All photometric data observed in 2017 confirmed the excited rotation state of 2012 TC4 with a main period of 12.2 minutes.

Here we revisit the situation using more sophisticated methods and tools. We reconstruct the convex shape model and spin state of 2012 TC4 from the available light curves that include the published data in the literature and our own new observations. We show that the rotation state must have changed between the 2012 and 2017 apparitions, and we propose a Yarkovsky–O’Keefe–Radzievskii–Paddack (YORP)-driven spin evolution as the most likely explanation. The data are described in Section 2, the physical model of the body is developed in Section 3, and the theoretical analysis of rotation dynamics is given in Section 4. Mathematical methods and the numerical setup of the theoretical model are summarized in Appendix A. The best fit of our physical model to the available light curves is shown in Appendix B.

2. Optical Photometry Data

To reconstruct the spin state of 2012 TC4, we collected its light curves observed during both close approaches. Photometric observations from 2012 and 2017 were made using a variety of telescopes having apertures between 0.35 and 5 m and equipped with CCD cameras. Observational circumstances with references to original sources are listed in Table 1. Apart from previously published light curves, our data set also includes several new observations (indicated by coauthor names in the last column). In particular, we obtained four light curves using the Pistoiese 0.6 m telescope (MPC code: 104) with the CCD Apogee U6, which has a

Table 1
Observation Details (New Data Denoted by Name of a Coauthor)

Telescope	Date (UT)	Filter	References
2012			
OAVdA 0.81 m (Italy)	2012 10 09.9	C	Carbognani (2014)
Pistoiese 0.6 m (Italy)	2012 10 09.9	R	Bacci
Pistoiese 0.6 m (Italy)	2012 10 10.0	R	Bacci
MRO 2.4 m (USA)	2012 10 10.2	V	Ryan & Ryan (2017)
Wise Observatory 0.72 m (Israel)	2012 10 10.8	V	Polishook (2013)
OAVdA 0.81 m (Italy)	2012 10 10.8	C	Carbognani (2014)
PROMPT1 0.41 m (Chile)	2012 10 11.1	Lum	Pollock
MRO 2.4 m (USA)	2012 10 11.1	V	Ryan & Ryan (2017)
PDO 0.35 m (USA) ^a	2012 10 11.2	V	Warner (2013)
2017			
Kitt Peak Mayall 4 m (USA)	2017 09 13.2	R	Reddy et al. (2019)
Kitt Peak Mayall 4 m (USA)	2017 09 14.1	R	Reddy et al. (2019)
Palomar Hale 5 m (USA)	2017 09 17.4	SR	Reddy et al. (2019)
Palomar Hale 5 m (USA)	2017 09 20.2	SR	Warner (2018)
SOAR 4.1 m (Chile)	2017 10 06.2	SR	Reddy et al. (2019)
PDO 0.35 m (USA)	2017 10 09.2	V	Warner (2018)
MRO 2.4 m (USA)	2017 10 09.2	V	Reddy et al. (2019)
Kiso 1.05 m (Japan)	2017 10 09.5	SG	Urakawa et al. (2019)
Wise Observatory 0.72 m (Israel)	2017 10 09.8	V	Reddy et al. (2019)
LCO-C 1 m (Chile)	2017 10 10.1	SR, SI	Reddy et al. (2019)
LCO-A 1 m (Chile)	2017 10 10.1	SR	Reddy et al. (2019)
PDO 0.35 m (USA)	2017 10 10.2	V	Warner (2018)
Nayoro 0.4 m (Japan)	2017 10 10.4	V	Urakawa et al. (2019)
BSGC 1 m (Japan)	2017 10 10.6	SG, SR, SI, SZ	Urakawa et al. (2019)
Lulin 1 m (Taiwan) ^b	2017 10 10.6	BVRI (diff.)	Lin et al. (2019)
Kiso 1.05 m (Japan)	2017 10 10.5	SG	Urakawa et al. (2019)
Wise Observatory 0.72 m (Israel)	2017 10 10.8	V	Reddy et al. (2019)
Pistoiese 0.6 m (Italy)	2017 10 10.9	R	Bacci
KMTNet 1.6 m (South Africa)	2017 10 10.9	V	Reddy et al. (2019)
Pistoiese 0.6 m (Italy)	2017 10 11.0	R	Bacci
USNA 0.51 m (USA)	2017 10 11.0	V	Reddy et al. (2019)
MRO 2.4 m (USA)	2017 10 11.1	R	Reddy et al. (2019)
PDO 0.35 m (USA)	2017 10 11.2	V	Warner (2018)
Kiso 1.05 m (Japan) ^c	2017 10 11.5	SG	Urakawa et al. (2019)
Lulin 1 m (Taiwan) ^b	2017 10 11.6	BVRI (diff.)	Lin et al. (2019)
Anan Science Center 1.13 m (Japan) ^c	2017 10 11.6	V	Urakawa et al. (2019)
Wise Observatory 0.72 m (Israel)	2017 10 11.8	V	Reddy et al. (2019)
AIRA 0.38 m (Romania)	2017 10 11.8	V	Sonka et al. (2017)
Wildberg Observatory 0.35 m (Germany) ^d	2017 10 11.8		Apitzsch
KMTNet 1.6 m (South Africa)	2017 10 11.9	V	Reddy et al. (2019)
MRO 2.4 m (USA)	2017 10 12.1	R	Reddy et al. (2019)

Notes. OAVdA: Astronomical Observatory of the Autonomous Region of the Aosta Valley; MRO: Magdalena Ridge Observatory; PROMPT1: Panchromatic Robotic Optical Monitoring and Polarimetry Telescopes; PDO: Palmer Divide Observatory; SOAR: Southern Astrophysical Research; LCO: Las Cumbres Observatory; BSGC: Bisei Spaceguard Center; KMTNet: Korea Microlensing Telescope Network (Kim et al. 2016); USNA: United States Naval Observatory; AIRA: Astronomical Institute of the Romanian Academy.

^a Split into six parts, each using different comparison stars.

^b These data were estimated by subtracting the average magnitudes of the comparison stars.

^c Split into two parts because we noted a possible calibration issue.

^d Split into two parts, each using different comparison stars.

35' × 35' field of view corresponding to a pixel scale of 2'' pixel⁻¹ in both apparitions. The raw frames were processed for the dark and flat-field correction, and the light curves of this observatory were constructed using Canopus software (Warner 2006). The preprocessing and photometry of the light curve observed at Wildberg Observatory (MPC code: 198) using a 0.35 m telescope equipped with an SXVF-H16 2048 × 2048 CCD camera were conducted using Astrometrica version 4.10.2.433 (Raab 2012). In the preprocess for these data, both dark and flat-field corrections were carried out. All photometric data were calibrated by referring to the PPMXL Catalog. (Roeser et al. 2010).

The Panchromatic Robotic Optical Monitoring and Polarimetry Telescopes (PROMPT), located at the Cerro Tololo Inter-American Observatory (CTIO) in Chile, consist of six 0.41 m reflectors equipped with the Apogee Alta U47+E2V camera. The field of view is 10' × 10' with 0.''59 pixel⁻¹. All raw image frames were processed (master dark, master flat, bad-pixel correction) using the software package MIRA. Aperture photometry was then performed on the asteroid and three comparison stars. A master image frame was created to identify any faint stars in the path of the asteroid. Data from images with background contamination stars in the asteroid's path were then eliminated.

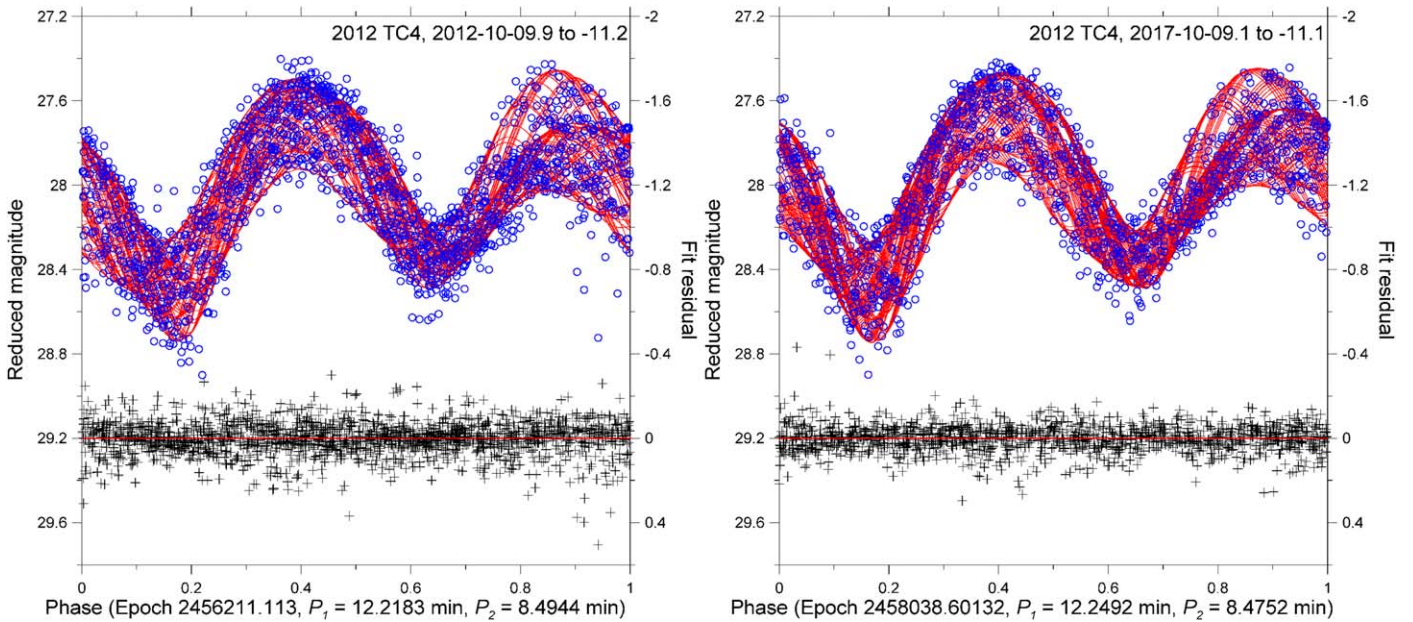


Figure 1. The blue open circles are the photometric data of 2012 TC4 taken from 2012 October 9.9 to 2012 October 11.2 (left) and from 2017 October 9.1 to 2017 October 11.1 (right) reduced to the unit geo- and heliocentric distances and a consistent solar phase (see text for details), folded with the respective main periods P_1 . The red curve is the best-fit fourth-order Fourier series with the two periods. The black plus signs are the postfit residuals (see the right ordinates).

A part of the published light curves was obtained from the Asteroid Lightcurve Data Exchange Format database (ALCDEF¹⁰; Warner et al. 2011). We also acquired the light curve published by Reddy et al. (2019) from the International Asteroid Warning Network (IAWN) 2012 TC4 Observing Campaign homepage.¹¹

Since the corrected light curves were observed using various filters and include both the relative and the absolutely calibrated observations, they have a magnitude offset between each other. As a result, the whole data set is primarily treated as an ensemble of relative light curves.

2.1. Two-period Fourier Series Analysis

In the first step, we analyzed the photometry data from 2012 and 2017 using the two-period Fourier series method (Pravec et al. 2005, 2014). Concerning the 2012 observations, we used all but one photometric light-curve series taken from 2012 October 9.9 to 2012 October 11.2 (see Table 1). In particular, we excluded the data taken on 2012 October 10.7 by Polishook (2013), where we found a possible timing problem.¹² Concerning the 2017 observations, we used a selected subset of the data taken between 2017 October 9.1 and 2017 October 11.1. This choice was motivated by noting that the observing geometry during this time interval in 2017 was very similar (due to the fortuitous resonant return of the asteroid to Earth after 5 yr) to the geometry of the time interval of the 2012 observations. This choice minimizes the possible (but anyway small) systematic effects due to changes in observing geometry

when comparing the results of our analysis of the data from the two apparitions (see below).

We reduced the data to the unit geo- and heliocentric distances and a consistent solar phase using the $H-G$ phase relation assuming $G = 0.24$, converted them to flux units, and fitted them with the fourth-order two-period Fourier series. A search for periods quickly converged, and we found the two main periods $P_1 = 12.2183 \pm 0.0002$ and $P_2 = 8.4944 \pm 0.0002$ minutes in 2012 and $P_1 = 12.2492 \pm 0.0001$ and $P_2 = 8.4752 \pm 0.0001$ minutes in 2017. The phased data and best-fit Fourier series, together with the postfit residuals, are plotted in Figure 1. We note that the smaller formal errors of the periods determined from the 2017 data were due to the higher quality of the 2017 observations (the best-fit rms residuals were 0.081 and 0.065 mag for the 2012 and 2017 data, respectively; see also the postfit residuals plotted in the bottom part of Figure 1). As for possible systematic errors of the determined periods, the largest could be due to the so-called synodic effect. It is caused by the change of position of a studied asteroid with respect to the Earth and Sun in the inertial frame during the observational time interval. An estimate of the magnitude of the synodic effect can be obtained using the phase-angle-bisector approximation, for which we used Equation (4) from Pravec et al. (1996). Using this approach, we estimate the systematic errors of the determined periods $\Delta P_1 = 0.0005$ and 0.0002 minutes and $\Delta P_2 = 0.0002$ and 0.0001 minutes in 2012 and 2017, respectively. These systematic errors are only slightly larger than the formal errors given above. A caveat is that the formula of Equation (4) in Pravec et al. (1996) was determined for the case of a principal-axis rotator. An exact estimate of the systematic period uncertainties due to the synodic effect for a tumbling asteroid would require an analysis of its actual non-principal-axis rotation in a given observing geometry, but we did not pursue it here, as the effect was naturally surmounted by the physical modeling presented in the next section.

¹⁰ <http://alcdef.org/>

¹¹ https://2012tc4.astro.umd.edu/Lightcurve/supplement/2012TC4_Lightcurve_Observations_Summary.html

¹² Indeed, D. Polishook (2020, personal communication) checked his data upon our request and confirmed that there was an issue with the times in his 2012 observations. We then used the corrected data for physical model reconstruction in Section 3.

As will be shown in the next section, the strongest observed frequency in the light curve, P_1^{-1} , is actually a difference between the precession and the rotation frequency of the tumbler: $P_1^{-1} = P_\phi^{-1} - P_\psi^{-1}$. The second-strongest frequency, P_2^{-1} , is then the precession frequency, P_ϕ^{-1} . This is a characteristic feature of the light curve of a tumbling asteroid in short-axis mode (SAM; see below). We note that the same behavior was observed for (99942) Apophis and (5247) Krylov, which are also in SAM (Pravec et al. 2014; Lee et al. 2020).

The principal light-curve periods P_1 and P_2 determined from the 2012 and 2017 observations differ at a high level of significance, formally on the order of about 100σ . While the systematic errors due to the synodic effect could decrease the formal significance by a factor of a few, the significance of the observed period changes would still remain large, on the order of several tens of σ . To interpret these findings in more depth, we turned to construct a physical model of 2012 TC4 as a tumbling object in the next section.

3. Physical Model

3.1. Model from 2017 Data

The light-curve data set from 2017 is much richer than that from 2012, so we started with the inversion of the 2017 data. We investigated possible frequency combinations based on the fact that the main frequencies f_1 and f_2 of a tumbling asteroid light curve are usually found at $2f_\phi$ and $2(f_\phi \pm f_\psi)$ or low harmonics and combination, where f_ϕ is the precession and f_ψ is the rotation frequency, respectively, and the plus sign is for long-axis mode (LAM) and the minus sign for SAM (Kaasalainen 2001). Using the values $f_1 = 4.898$ and $f_2 = 7.079 \text{ hr}^{-1}$ from the previous section, we found eight possible frequency combinations: $f_1 = f_\phi$, $f_2 = 2(f_\phi - f_\psi)$ (SAM1); $f_1 = 2(f_\phi - f_\psi)$, $f_2 = 2f_\phi$ (SAM2); $f_1 = 2(f_\phi - f_\psi)$, $f_2 = f_\phi$ (SAM3); $f_1 = f_\phi - f_\psi$, $f_2 = f_\phi$ (SAM4); $f_1 = 2f_\phi$, $f_2 = 2(f_\phi + f_\psi)$ (LAM1); $f_1 = 2f_\phi$, $f_2 = f_\phi + f_\psi$ (LAM2); $f_1 = f_\phi$, $f_2 = (f_\phi + f_\psi)$ (LAM3); and $f_1 = f_\phi + f_\psi$, $f_2 = f_\phi$ (LAM4). Then we conducted the shape and spin optimization for these combinations in the same way as in Lee et al. (2020). It was found that only the SAM4 solution provided an acceptable fit to the data and was physically self-consistent.

We used 34 light curves from 2017 October. Four light curves from 2017 September were very noisy and did not further constrain the model, so we did not include them in our analysis. We inverted the light curves with the method and code developed by Kaasalainen (2001) combined with Hapke's light-scattering model (Hapke 1993). According to Reddy et al. (2019), the colors of TC4 are consistent with the C or X complex; also, its spectrum is X type, with Xc type being the best match. The X complex contains low- and high-albedo objects, but the E type seems most likely because the high circular polarization ratio suggests that TC4 is optically bright (Reddy et al. 2019). This is in agreement with Urakawa et al. (2019), who also reported X-type colors. As a result, we used Hapke's model with parameters derived for E-type asteroid (2867) Šteins (Spjuth et al. 2012): $\varpi = 0.57$, $g = -0.30$, $h = 0.062$, $B_0 = 0.6$, and $\bar{\theta} = 28^\circ$. Because our data did not cover low solar phase angles, the h and B_0 parameters for the opposition surge and also roughness $\bar{\theta}$ were fixed. We optimized the ϖ and g parameters, and they converged to values of $\varpi = 0.69$, $g = -0.20$, which gave a geometric albedo of 0.34. An alternative solution with fixed values $\varpi = 0.57$, $g = -0.30$

provided an only marginally worse fit, and the kinematic parameters were not affected. In general, the solution of our inverse problem was not sensitive to Hapke's parameters like in previous studies (e.g., Scheirich et al. 2010; Pravec et al. 2014; Lee et al. 2020).

The rotation and precession periods had the following values: $P_\psi = 27.5070 \pm 0.002$ and $P_\phi = 8.47512 \pm 0.0002$ minutes, respectively. The 1σ uncertainties were estimated from the increase of χ^2 when varying the solved-for parameters; given a number of measurements of about 8600, the 3σ uncertainty interval corresponds to an about 5% increase in χ^2 (e.g., Vokrouhlický et al. 2017). The direction of the angular momentum vector in ecliptic coordinates was $\lambda = 92^\circ$, $\beta = -89.6^\circ$, practically oriented toward the south ecliptic pole. Normalized moments of inertia were $I_1 = 0.41$, $I_2 = 0.81$, but the model was not too sensitive to their particular values. The inertia moments computed from the 3D shape (assuming constant density) were $I_1 = 0.435$, $I_2 = 0.831$, indicating consistency with the kinematic parameters above.

The dark facet, which is always introduced into a convex shape model to regularize the solution (Kaasalainen & Torppa 2001), represented about a few percent of the total surface area, and forcing it to smaller values led to a worse fit. This might mean that there is some albedo variation on the surface of TC4 or that its real shape is highly nonconvex and a convex-shape approximation has its limits.

3.2. Model from 2012 Data

For this model, we used 14 light curves from 2012. The rotation and precession periods were now $P_\psi = 27.873 \pm 0.005$ and $P_\phi = 8.4945 \pm 0.0003$ minutes, respectively. The 1σ uncertainties were estimated in the same way as for the 2017 model, namely, from the increase of χ^2 . The direction of the angular momentum vector was $\lambda = 89^\circ$, $\beta = -90^\circ$, with moments of inertia $I_1 = 0.43$, $I_2 = 0.80$. The 3D shape model was similar to that reconstructed from 2017 data, and the direction of the angular momentum vector was practically the same.

In spite of consistency in all other solved-for parameters, we thus observed that the periods P_ϕ and P_ψ for the two apparitions were significantly different. Attempts to use the 2017 values to fit the 2012 data, or vice versa, led to a dramatically worse fit. We scanned the period parameter space around the best-fit values and plotted the relative χ^2 values; see Figure 2. The minima in χ^2 for the 2012 and 2017 periods are clearly separated.

3.3. Model from 2012 and 2017 Data

The 3D models reconstructed from the two apparitions independently have similar global shapes, but their details are different (Figure 3). If we take the shape reconstructed from the 2017 data and use it to fit the 2012 data, it gives a satisfactory fit to the light curves. However, a better way to use all data together is not to treat them separately but to instead invert both apparitions together with a common shape model that would differ only in kinematic parameters. Therefore, we modified the original inversion code of Kaasalainen (2001) to enable including two independent light-curve sets. We assumed that the only parameters that were different for the two apparitions were the rotation and precession periods P_ψ , P_ϕ and initial Euler angles ϕ_0 , ψ_0 . The parameters describing the shape and the direction of the angular momentum vector were the same. So the full set of kinematic parameters for a two-apparition

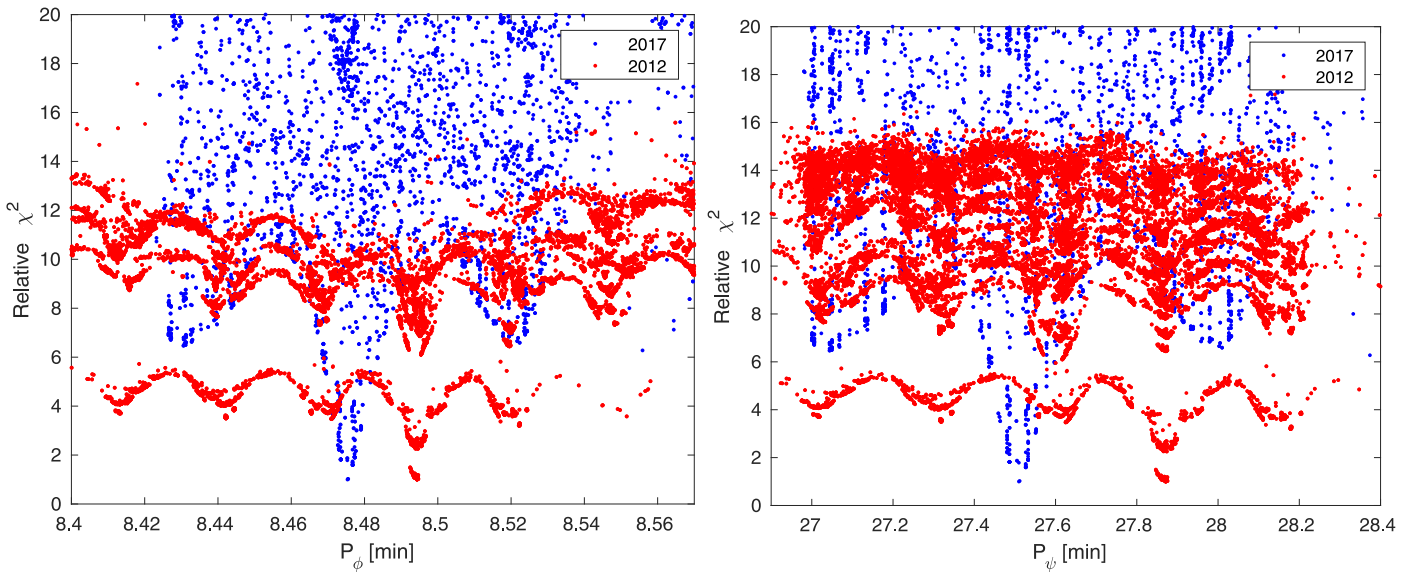


Figure 2. Period scan for data from 2017 (October only) and 2012. Each point represents one trial model that converged to given P_ϕ , P_ψ , and χ^2 values. Minima for the 2012 and 2017 data are clearly separated. The relative χ^2 was normalized to have a minimum value of 1.

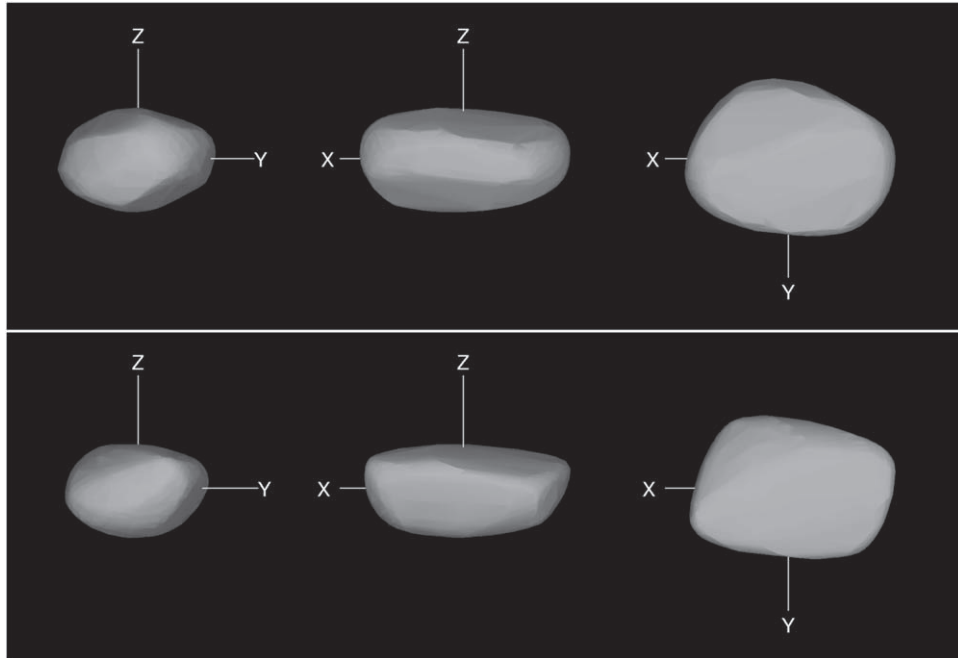


Figure 3. Shape models reconstructed independently from 2012 (top) and 2017 (bottom) light curves. The 2017 model is almost identical to that reconstructed from joint inversion of 2012 and 2017 data.

model was $(\lambda, \beta, \phi_0^{(1)}, \phi_0^{(2)}, \psi_0^{(1)}, \psi_0^{(2)}, P_\psi^{(1)}, P_\psi^{(2)}, P_\phi^{(1)}, P_\phi^{(2)}, I_1, I_2)$, where the superscript (1) is for the 2012 apparition and (2) is for the 2017 apparition. The two light-curve data sets were independent in the sense that the integration of kinematic equations (Equation (A.3) in Kaasalainen 2001) was done separately for 2012 and 2017 data; the two epochs were not directly connected. The final model shape is almost identical to that reconstructed from only 2017 data shown in Figure 3. The fit of the final model to individual light curves is shown in Appendix B. Rotation and precession periods converged to practically the same values as with the independent treatment of each of the two apparitions. The best-fit parameters for the 2012 and 2017 apparitions are listed in Table 2. The physical models of 2012 TC4 from 2012 and 2017 and the light-curve

data set used to reconstruct these models are available from the DAMIT database¹³ (Ďurech et al. 2010).

3.4. Bootstrap

To estimate the uncertainties of physical periods and further robustly demonstrate that their change between 2012 and 2017 is significant, we created bootstrapped data samples and repeated the light-curve inversion for them. From both the 2012 and 2017 data sets, we created 1000 bootstrap samples by randomly selecting the same number of light curves from the original data set. For the 2017 October bootstrap, 279 final shape models had a clearly

¹³ <https://astro.troja.mff.cuni.cz/projects/damit/>

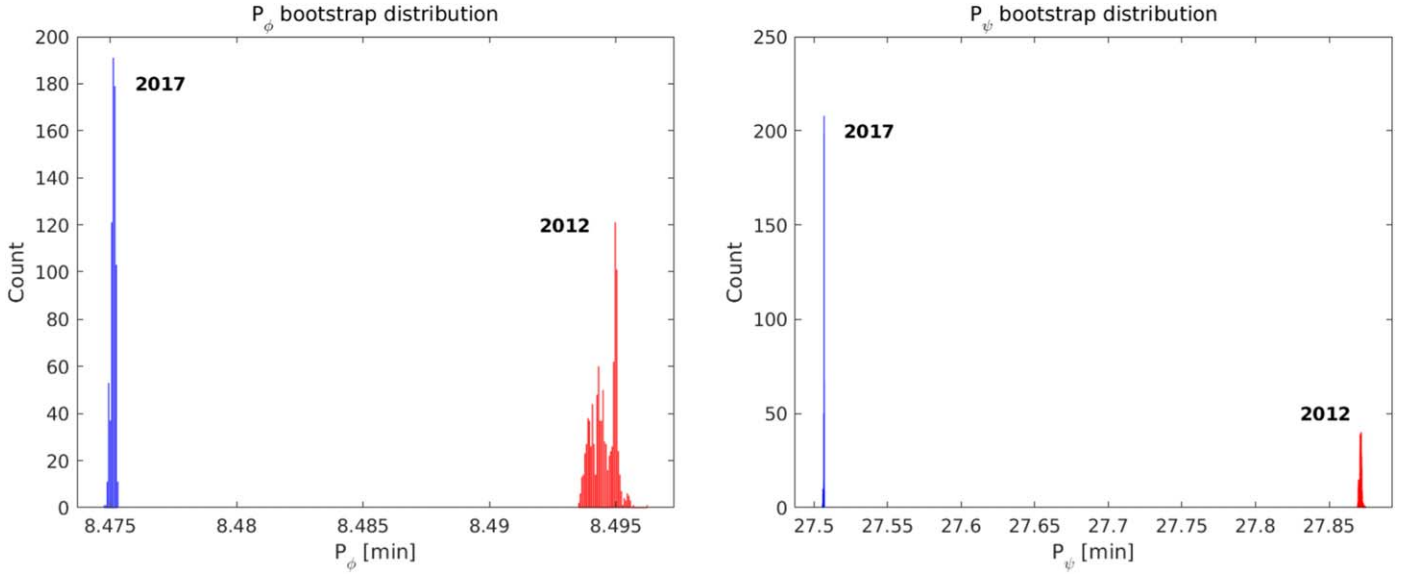


Figure 4. Distribution of periods P_ϕ (left) and P_ψ (right) for bootstrapped light curves.

Table 2

Parameters of the Model in Figure 3 Reconstructed from 2012 and 2017 Light Curves

	2012	2017
P_ψ (minutes)	27.8720 ± 0.0007	27.5070 ± 0.0002
P_ϕ (minutes)	8.4944 ± 0.0005	8.47511 ± 0.00008
ϕ_0 (deg)	322 ± 8	74 ± 9
ψ_0 (deg)	198 ± 0.02	180 ± 0.2
JD ₀	2,456,210.00	2,458,032.69
λ (deg)	103 ± 78	
β (deg)	-88.5 ± 0.7	
I_1	0.42	
I_2	0.81	
w	0.67	
g	-0.20	
h	0.062	
B_0	0.6	
$\bar{\theta}$ (deg)	28	
$\delta L/L$	0.00078 ± 0.00006	
$\delta E/E$	-0.0035 ± 0.0001	

Note. The reported errors correspond to standard deviations of parameters computed from bootstrap models. Parameters without errors were fixed (Hapke’s parameters) or did not change (I_1 and I_2). The formally small uncertainty of ψ_0 means that this initial orientation angle is correlated with the shape and does not change significantly with different bootstrap data sets. Parameter λ is practically unconstrained because the angular momentum direction is very close to $\beta = -90^\circ$. Values $\delta L/L$ and $\delta E/E$ are relative changes of angular momentum L and energy E between 2012 and 2017, i.e., $\delta L/L = (L_{2017} - L_{2012})/L_{2017}$ and $\delta E/E = (E_{2017} - E_{2012})/E_{2017}$.

wrong inertia tensor that was not consistent with the kinematic I_1 , I_2 parameters, so we removed them from the analysis. For all remaining bootstrap models, we plot histograms of P_ϕ and P_ψ distribution in Figure 4. The standard deviations of the precession period P_ϕ are 0.0005 and 0.00009 minutes for the 2012 and 2017 data, respectively, which are similar to the uncertainty values derived in Sections 3.1 and 3.2. For the rotation period P_ψ , these standard deviations are 0.0008 and 0.0002 minutes, which is significantly smaller than our χ^2 -based estimate. Nevertheless, the

difference between periods determined from the 2012 and 2017 apparitions is much larger than their uncertainty intervals, and we are not aware of any random or model errors that could cause such a difference. Our conclusion is that the spin state of TC4 has changed from 2012 to 2017, and the rotation and precession periods have decreased. In what follows, we try to interpret this change using a theoretical model of TC4 spin evolution with the relevant torques.

4. Theory

4.1. Orbital Dynamics

The unique observational opportunities of 2012 TC4 are directly related to its exceptional orbit. The asteroid had a deep encounter with Earth on 2012 October 12, during which the closest distance to the geocenter was approximately 95,000 km (Figure 5). However, the more unusual circumstance was that the 2012 close encounter resulted in a change of 2012 TC4’s orbital semimajor axis that placed it nearly exactly at the 5:3 resonance with Earth’s heliocentric motion. As a result, 5 yr after the first close encounter, i.e., on 2017 October 12, the relative configuration of the asteroid and Earth nearly exactly repeated, again placing it in a deep encounter configuration. This time, the closest approach to the geocenter had an even closer distance of 50,200 km. Astrometric observations during the two close approaches, including Arecibo and Green Bank radar data taken in 2017, allowed a very accurate orbital solution over the 5 yr period of time in between 2012 and 2017. In the context of this paper, we note that it also provided interesting information about the nongravitational effects that need to be empirically included in orbit determination. Adopting a methodology from cometary motion (e.g., Marsden et al. 1973 and Farnocchia et al. 2013 or Mommert et al. 2014 for the asteroidal context), we note the following values of radial A_1 and transverse A_2 accelerations: (i) $A_1 = (2.17 \pm 0.80) \times 10^{-11}$ au day $^{-2}$, or $(4.35 \pm 1.60) \times 10^{-10}$ m s $^{-2}$, and (ii) $A_2 = -(2.73 \pm 0.65) \times 10^{-13}$ au day $^{-2}$ (both assume $\propto r^{-2}$ heliocentric decrease; see the JPL/Horizons webpage, <https://ssd.jpl.nasa.gov/sbdb.cgi>). At first sight, these values appear very reasonable (compare with, e.g., A_1 and A_2 fits for the $\simeq 4$ m body 2009 BD; Mommert et al. 2014; Vokrouhlický et al. 2015a).

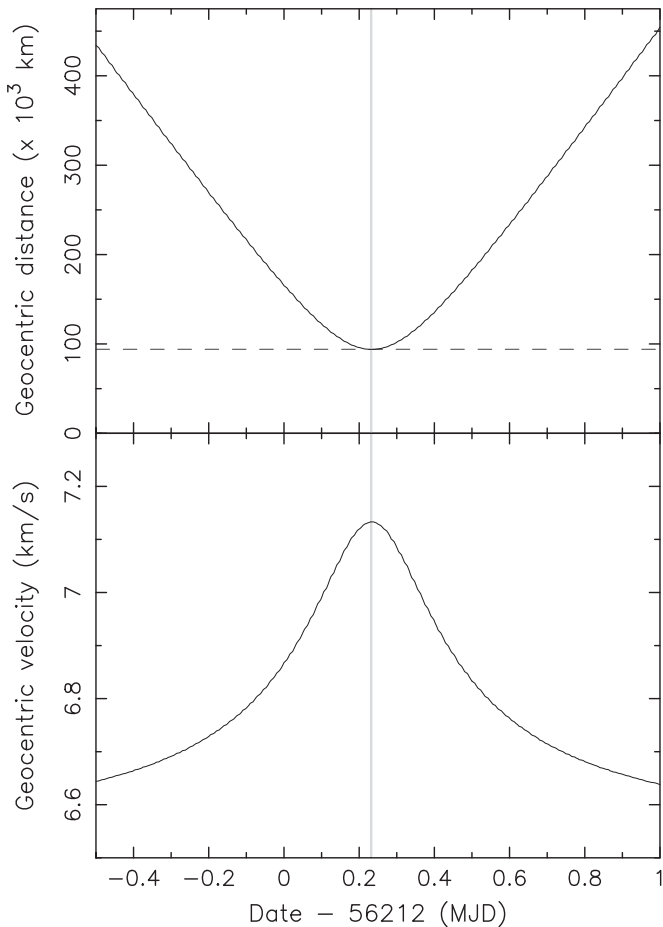


Figure 5. Geocentric distance (top) and relative velocity (bottom) of 2012 TC4 during its close encounter with Earth on 2012 October 12 (nominal minimum configuration at MJD 56,212.229; gray vertical line); the abscissa shows the time in days with respect to MJD 56,212. The dashed horizontal line in the top panel shows the minimum distance of $\simeq 95,000$ km. The asymptotic value of the relative velocity with respect to Earth, $\simeq 6.5$ km s $^{-1}$, increases to more than 7.1 km s $^{-1}$ by Earth’s gravity.

If we were to interpret both components as a result of radiation forces, we might further obtain useful information about the body. The radial component would represent the direct solar radiation pressure. In a simple model, where we assume a spherical body of size D and bulk density ρ , we have $A_1 \simeq 3C_R F_0 / (2\rho Dc)$, with C_R the radiation pressure coefficient (dependent on sunlight scattering properties on the surface), $F_0 \simeq 1367$ W m $^{-2}$ the solar constant, and c the light velocity. Adopting $C_R \simeq 1.2$ and $D \simeq 10$ m, we obtain a very reasonable bulk density $\rho \simeq (1.9 \pm 0.7)$ g cm $^{-3}$. The transverse component of nongravitational orbital effects makes sense when interpreted as the Yarkovsky effect (e.g., Vokrouhlický et al. 2015a). Note that the abovementioned value of A_2 translates to a secular change of the semimajor axis $da/dt = -(110 \pm 26) \times 10^{-4}$ au Myr $^{-1}$ (see, e.g., Farnocchia et al. 2013). Given the near extreme obliquity of the rotational angular momentum, we may safely restrict to the diurnal component of the Yarkovsky effect. The negative value of A_2 , or da/dt , corresponds well to the retrograde sense of 2012 TC4 rotation (implied by the direction of the rotational angular momentum vector; Section 3). Next, borrowing the simple model for a spherical body from Vokrouhlický (1998) and fixing the size $D = 10$ m, the inferred bulk density $\rho \simeq 1.9$ g cm $^{-3}$, and the surface thermal conductivity $K = 0.05$ W m $^{-1}$ K $^{-1}$, we estimate that the corresponding surface

thermal inertia is $\Gamma \simeq 490^{+270}_{-250}$ in SI units (though we note that there is also a lower-inertia solution possible, like in Mommert et al. 2014). This is a very adequate value too (e.g., Delbó et al. 2015). Obviously, due to the many frozen parameters in the model (and its simplicity), the realistic uncertainty in Γ would be larger. However, it is not our intention to fully solve this problem. We satisfy ourselves with the observation that the needed empirical nongravitational accelerations in the orbital fit may be very satisfactorily interpreted as radiation-related effects. In the next sections, we show that the change in the rotation state between the 2012 and 2017 observation epochs may be very well explained by the radiation torque known as the YORP effect (e.g., Vokrouhlický et al. 2015a).

4.2. Rotational Dynamics

Our methods and mathematical approach used to describe the evolution of the rotation state of 2012 TC4 are presented in Appendix A; therefore, here we provide just a general outline. We numerically integrated Euler Equations (A2) and (A4) describing the spin state evolution of 2012 TC4 in between the observation runs in 2012 and 2017. The kinematical part, describing the transformation between the inertial frame and the body frame defined by the principal axes of the tensor of inertia, was parameterized by the Rodrigues–Hamilton parameters $\lambda = (\lambda_0, \lambda_1, \lambda_2, \lambda_3)$ (see, e.g., Whittaker 1917). This choice helps to remove problems related to coordinate singularity given by the zero value of the nutation angle. The dynamical part is represented by the evolution of the angular velocity ω in the body frame. Note that in most cases of asteroid light-curve interpretation, a simplified model of a free top would be sufficient (also used in Section 3 to fit the 2012 and 2017 data separately). However, the evidence of the change of the rotation state of 2012 TC4 in between the 2012 and 2017 epochs, discussed above, requires appropriate torques to be included in the model. We addressed two effects:

1. gravitational torques due to the Sun and Earth and
2. radiation torques due to the sunlight scattered by the surface and thermally reradiated (the YORP effect; e.g., Bottke et al. 2006; Vokrouhlický et al. 2015a).

The tidal gravitational fields of the Sun and the Earth were represented in the body frame using the quadrupole approximation (Equation (A7); e.g., Fitzpatrick 1970; Takahashi et al. 2013). The nature of the perturbation is different for the Sun and Earth. In the solar case, the gravitational torque results in a small tilt of less than 1’ describing a small segment on the precession cone. The effect of the Earth-induced gravitational torques manifests as an impulsive effect only during close encounters. Our main goal was to verify that, due to the fast rotation of 2012 TC4, the effect averages out and cannot contribute to the observed change in rotational frequencies. Indeed, Figure 6 shows the change of the osculating rotational (intrinsic) angular momentum and energy during the 2012 close encounter with Earth (only about six times larger effects are observed during the closer encounter in 2017, but this is not relevant for our analysis anyway, because the observations preceded this approach). The initial data of the simulation were taken from the observations fit in 2012, namely, before the encounter. Recall that the characteristic timescale of the encounter is about half a day (determined, for instance, as a width of the characteristic Earth relative velocity increase in the bottom panel of Figure 5 at an $\simeq 6.8$ km s $^{-1}$ level, half the value between the asymptotic and peak velocities). In comparison,

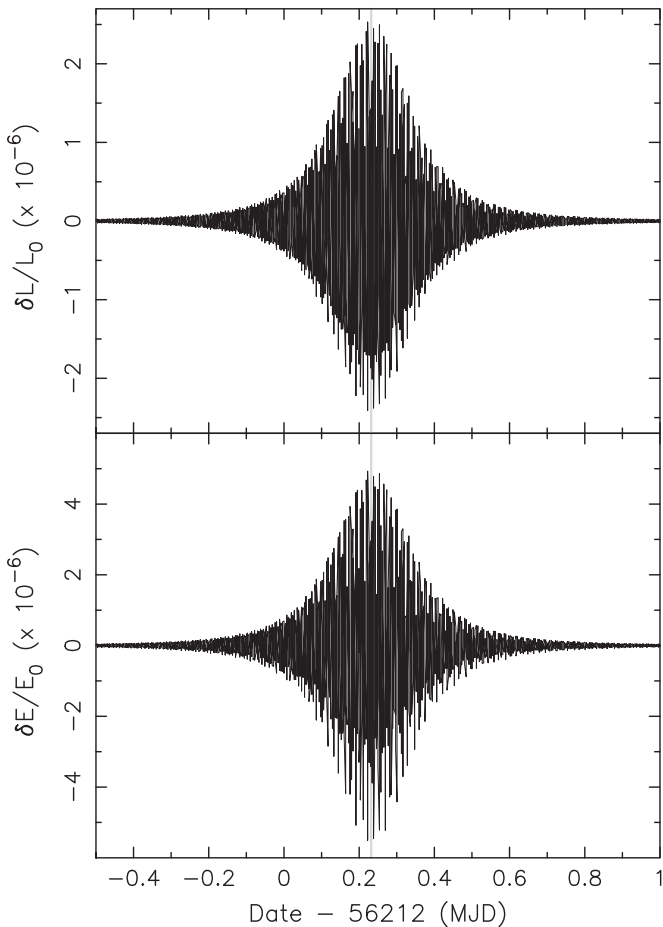


Figure 6. Effect of Earth’s gravitational torque in quadrupole approximation on the rotation state parameters of 2012 TC4 during its close encounter on 2012 October 12 (the gray line denotes the nominal minimum distance configuration). The abscissa shows the time in days with respect to MJD 56,212 (as in Figure 5). The upper panel shows a fractional change of the rotational angular momentum $\delta L = L - L_0$, normalized by the initial value L_0 , and the bottom panel shows a fractional change of the rotational energy $\delta E = E - E_0$, normalized by the initial value E_0 (note that both ordinate scales are in 10^{-6}). The resulting change of both parameters after the encounter is $\leq 5 \times 10^{-9}$.

the characteristic rotational periods P_ψ and P_ϕ are of the order of minutes, i.e., much shorter. As a result, the effect of Earth’s gravitational torque efficiently averages out during each of the rotation cycles (a significant effect may be expected only for very slowly rotating bodies and sufficiently deep encounters, such as seen for 4179 Toutatis during its 2004 close encounter with Earth; e.g., Takahashi et al. 2013). Therefore, we may conclude that the gravitational torques cannot explain the observed change in the rotation state of 2012 TC4 in between the 2012 and 2017 epochs. Still, we keep them in our model for the sake of completeness.

The radiation torques are of a quite different importance. It is well known that the YORP effect is able to secularly change the rotational frequency and tilt the rotational angular momentum in space. While mostly studied in the limit of a rotation about the shortest axis of the inertial tensor, generalizations to the tumbling situation were also developed. Both numerical (Vokrouhlický et al. 2007) and analytical (Cicalò & Scheeres 2010; Breiter et al. 2011) studies confirmed that the YORP effect is able to change rotational angular momentum, and its orientation, in both the inertial space and bodyframe in an appreciable manner. As usual, the effect is more important on small bodies. Here we included the simple,

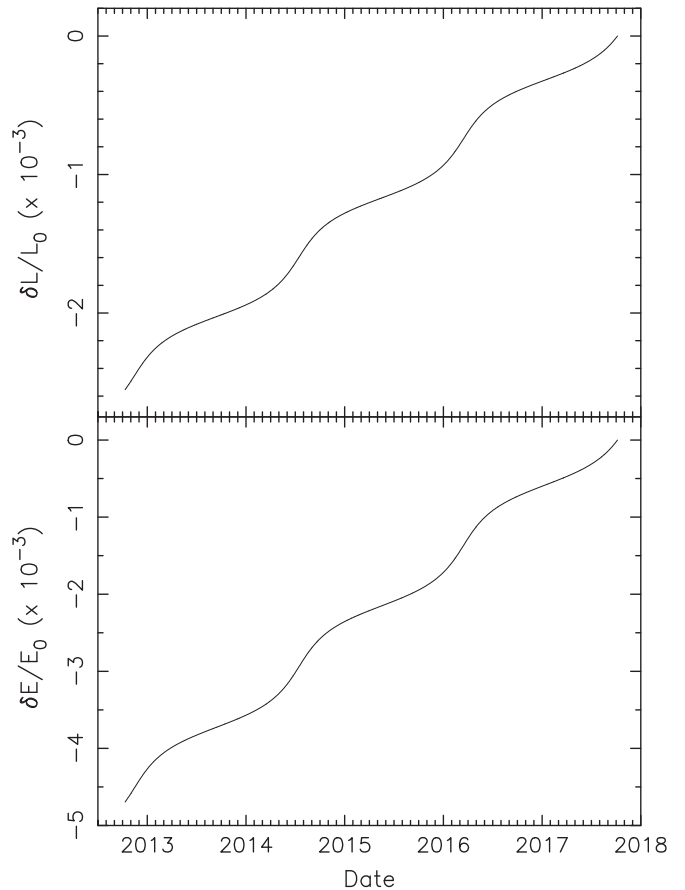


Figure 7. Effect of the radiation (YORP) torque on the rotation state parameters of 2012 TC4 in the time interval between the two recent close encounters with Earth (i.e., 2012 October 12 and 2017 October 12). The nominal model is used here to obtain a first insight into the expected order of magnitude of the perturbation. The abscissa shows time in years. The upper panel shows a fractional change of the rotational angular momentum $\delta L = L - L_0$ normalized by the initial value L_0 , and the bottom panel shows a fractional change of the rotational energy $\delta E = E - E_0$ normalized by the initial value E_0 (note that both ordinate scales are in 10^{-3}). Both reference values were taken at MJD 58,032.19, the mean epoch of the 2017 observations, and the asteroid’s rotation state was propagated backward in time to 2012 October.

zero-inertia limit developed in Rubincam (2000) and Vokrouhlický & Čapek (2002); see Equation (A8). A first look into the importance of the radiation torques may be obtained by taking the nominal solution of the rotation state from the 2017 observations, including the appropriate shape model, and propagating it backward in time to early 2012 October (the epoch of the first set of observations). We use the more accurate 2017 model as a reference, rather than the one constructed from the poorer 2012 observations. The length scale of the model was adjusted to correspond to an equivalent sphere of diameter $D = 10$ m, and the density was $\rho = 1.4 \text{ g cm}^{-3}$. We verified that the results have the expected invariance to rescaling of both ρ and D such that $\rho D^2 = \text{const}$. Our nominal choice of the 1.4 g cm^{-3} bulk density, albeit conflicting with the suggested E-type spectral classification of TC4, is therefore linked to the assumed equivalent size of 10 m, but it might be redefined according to the rescaling principle. This combination of parameters provides a very nice match of the P_ϕ period change due to our YORP model (see Section 4.3).

Figure 7 provides information about the secular change in the rotational angular momentum L (top) and energy E (bottom) in that simulation. Here we see a long-term change

in both quantities. The wavy pattern is due to the eccentricity of the 2012 TC4 orbit and a stronger YORP torque at perihelion. The accumulated fractional change in both L and E is a few times 10^{-3} . This is promising because the observed change in these quantities is of the same order of magnitude (see Table 2) and makes us believe that the change in the directly observable P_ψ and P_ϕ periods will also be as needed. Nevertheless, we also note a difference. The simulation results shown in Figure 7 indicate that both angular momentum and energy increased from 2012 to 2017. Such behavior is perhaps expected in the first place (for instance, in the case of a body in a principal-rotation state, YORP would necessarily affect both E and L in the same way). However, rotation state solutions from observations in 2012 and 2017 tell us something else (see Table 2): the rotational angular momentum L increased between 2012 and 2017, while the energy E decreased. Before commenting more on this difference, we first provide a more detailed analysis of the radiation torque effects for 2012 TC4 in our modeling, this time using the whole suite of acceptable initial data and shape models (all compatible with the observations; Section 3.4). This will allow a statistical assessment of the predicted values.

4.3. Results

An ideal procedure of proving that the observed changes in tumbling-state periods P_ϕ and P_ψ are due to the radiation (YORP) torques would require a highly reliable theoretical model (numerical propagation of 2012 TC4's rotation state with appropriate torques included) employed to fit all available observations (in our case, data from 2012 and 2017 October). Obviously, the only ‘‘comfort’’ of this analysis would be to possibly adjust some free (unknown) parameters. Unfortunately, such a plan is presently too ambitious; thus, we resort to a simpler way.

Recall the much easier situation when the YORP effect has been searched (and detected) for asteroids rotating in the lowest-energy mode, namely, about the shortest principal axis of the inertia tensor. In this case, YORP results in a secular change of the unique rotation period P (as in P_ϕ and P_ψ , when the body tumbles). The measurements are rarely precise enough, and the effect strong enough, to directly reveal the change in the period P (see, though, an exception for 54509 YORP; Lowry et al. 2007). More often, one uses the fact that the linear-in-time change in P produces a quadratic-in-time effect in the rotation phase. Properly linking the asteroid rotation phase over many observation sessions with an empirical quadratic term helps to characterize changes of P that are individually too small to be determined from one-apparition observations (see, e.g., Vokrouhlický et al. 2015a). This approach adopts an empirical magnitude of the quadratic term in the rotation phase and simply solves it as a free parameter (not combining it with a theoretical model at that stage). Interpretation in terms of the YORP effect is done only a posteriori, when the fitted amplitude of the phase-quadratic term is compared with a prediction from the YORP model. And even then, the comparison is often not simple, because the model prediction for YORP is known to depend on unresolved small-scale irregularities of the body shape. On several occasions, one has to be satisfied with a factor of a few difference accounting for the model inaccuracy.

Things are quite a bit more complex when the body tumbles. First of all, it is not clear how to set the empirical approach from

above and apply it in this situation. At the same time, the direct modeling approach is probably even less accurate than in the case of rotation about the principal axis of the inertia tensor. Not only does the worry about the role of unresolved small-scale irregularities remain, but the present YORP model is restricted to the zero thermal conductivity limit (see, e.g., Vokrouhlický et al. 2007 for the numerical approach and Cicalò & Scheeres 2010 and Breiter et al. 2011 for analytical studies). The Yarkovsky acceleration for tumblers was evaluated with thermal models (e.g., Vokrouhlický et al. 2005, 2015b), but in these cases, P_ϕ and P_ψ were slightly tweaked to make them resonant (an approach we cannot afford here). In this situation, we adopted the following simple procedure.

4.3.1. Model Based on 2017 Data

We start with a set of models uniquely based on the most reliable and accurate observations from the 2017 apparition. In particular, we constructed 687 variants of the 2012 TC4 physical model (Section 3.1). They are all very similar because they sample tight parameter variations, all resulting in acceptable fits of the data. These represent (i) slightly modified initial rotation parameters (Euler angles and their derivatives, as well as the inertial space direction of the rotational angular momentum vector) and (ii) slight shape variants of the body. The initial epoch MJD 58,032.19 was common to all variant models. Using these initial data and shape models, we propagated all 687 clone realizations of 2012 TC4 backward in time to the epoch MJD 56,209.88, characteristic of the 2012 October observations. We used our numerical approach described above with both gravitational and radiation (YORP) torques included. For the latter, we assumed an effective size $D = 10$ m (corresponding to a sphere of the same volume of the models) and bulk density $\rho = 1.4$ g cm $^{-3}$. The abovementioned rescaling rule, namely, invariance to ρD^2 , may allow us to transform our results to other combinations of D and ρ values.

The evolutionary tracks of angular momentum L and energy E secular changes due to the YORP torques mostly resemble those from Figure 7. For some model variants, which were more different from the nominal one, the slope of the overall secular change in L and/or E was shallower or steeper. At the initial and final epochs of our simulations, we determined P_ϕ and P_ψ periods from a short numerical simulation of a free-top model. We also verified that the P_ψ values correspond exactly to those provided by the analytical formula (Equation (A5)). Figure 8 shows our results. The blue histograms are for the initial data, i.e., the 2017 October rotation state. Because the observations were numerous and of good quality, the model variants differ only slightly, and the P_ϕ and P_ψ distributions are tight (they also match those from Figure 4). The red histograms in Figure 8 were determined from the last epoch of our numerical runs and correspond to the predicted rotation state of 2012 TC4 in 2012 October. We note that both periods appreciably changed, as already anticipated from the preliminary simulation shown in Figure 7. These P_ϕ and P_ψ distributions are obviously less tight than the initial ones, reflecting the different evolutionary tracks of the individual clone variants. Our prime interest is to compare the red distribution in Figure 8 (from simulations) to the red distributions in Figure 4 (from the 2012 observations; also highlighted with a dashed line for the P_ϕ period). First, we note that the match of the P_ϕ periods is surprisingly good. The mean value of 8.495 minutes of the observations corresponds rather well to the mean value of 8.497 minutes of the simulated data, which have a comfortably

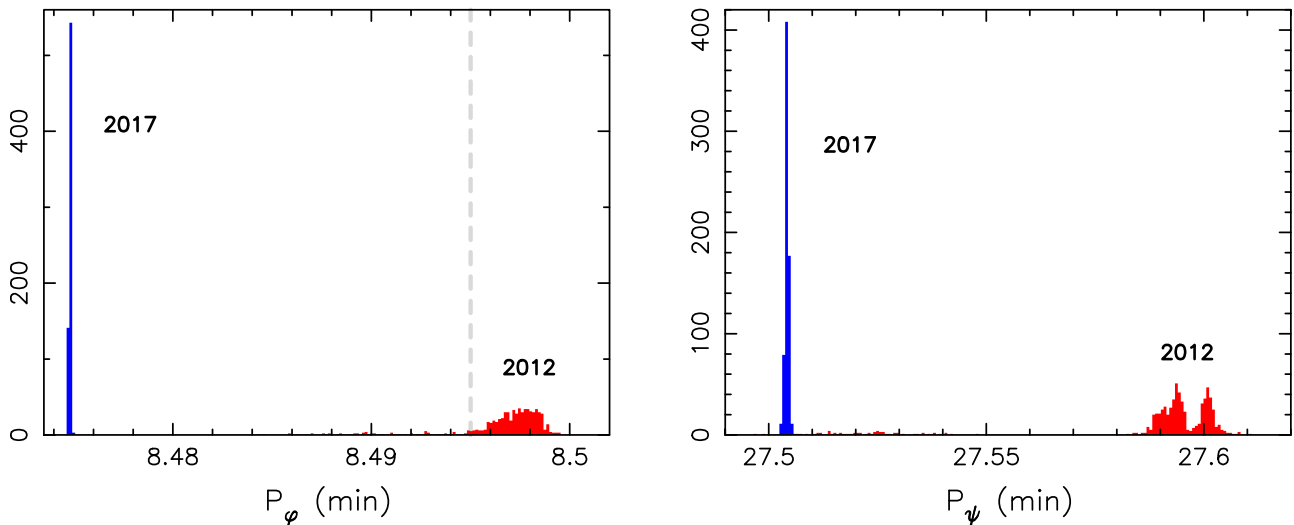


Figure 8. Distribution of periods P_ϕ (left) and P_ψ (right) for 687 models of 2012 TC4 from our numerical simulation containing both gravitational and radiation (YORP) torques. The individual models sample the possible initial orientation of the angular momentum vector \mathbf{L} in the inertial space, the orientation of the body frame in the inertial space, and slight shape variants of the body. All models were constructed using the 2017 October observations; therefore, they are referred to the common epoch MJD 58,032.19. Blue histograms are computed from these initial data, and they are identical to those in Figure 4. The red histograms correspond to the rotation state of 2012 TC4 at MJD 56,209.88, the nominal epoch of the 2012 October observations (the mean P_ϕ value from the observations is shown with a vertical dashed line). Unlike in Figure 4, the 2012 data here were computed from the spin state vectors obtained from our numerical propagation of the 2012 TC4 rotation starting in 2017 October.

large dispersion of 0.003 minutes to overlap with the observed data; in fact, the shift in P_ϕ is even larger than required. Interestingly, the comparison is not as good in the P_ψ period. The model-predicted value of 27.59 ± 0.02 minutes (formal uncertainty) is short to explain the observations, which provide, on average, 27.87 minutes. Still, the model indicates a significant shift from the initial value of 27.5070 ± 0.0002 minutes. Nevertheless, to reach the value from the 2012 observations, the shift would need to be about 3.7 times larger. We do not know the reason for this difference; in all likelihood, it is related to the misbehavior in the rotational energy evolution (see above). We suspect that the overly simple modeling of the YORP effect, such as the surface thermal inertia and/or the unresolved small-scale shape irregularities, plays an important role here (note that a factor of 3 between the observations and model prediction was also seen in the cases where YORP was detected for asteroids rotating about the principal axis of the inertia tensor). The fact that some deeper aspects of the model are not characterized well, as witnessed by the opposite sign of the energy evolution, implies that our results cannot be easily reconciled with the observations by a simple rescaling of size D and bulk density ρ . We have verified that the accumulated shifts in both the P_ϕ and P_ψ periods are proportional to ρD^2 . Thus, the P_ψ mismatch could be explained by assuming that 2012 TC4's size is $\simeq 5.2$ m, but this would produce a factor of $\simeq 3.7$ inconsistency in the P_ϕ period (making the modeled value larger than observed). Instead, we believe that some missing details of the YORP modeling, which result in different effects on P_ϕ and P_ψ , are responsible for the difference.

4.3.2. Model Based on a Combination of 2012 and 2017 Data

For the sake of comparison, we also repeated our analysis using models based on a combination of the observations in 2012 and 2017 (Section 3.3). Obviously, at each of these epochs, we considered different parameters of the rotation state, but now we enforce that the same shape model is used for both data sets. This solution gives us an opportunity to consider two sets of

initial conditions for our simulation, in both 2012 and 2017, and analyzes the predictions in the complementary epoch (integrating the rotation model once backward in time and once forward in time). Obviously, in all cases, our model includes the gravitational and radiation torques, $D = 10$ m effective size, and $\rho = 1.4 \text{ g cm}^{-3}$ bulk density, as before (needed for the evaluation of the radiation torques).

We start with the case of the initial data in 2017 October and backward-in-time integration. This is directly comparable with the results above, when only observations in 2017 were used. However, the models are slightly different in all aspects (initial conditions and shape) because now the 2012 observations play a role in their construction. The results are shown in Figure 9. While slightly different than in Figure 8, the principal outcome is the same: (i) a fairly satisfactory prediction for the P_ϕ period and (ii) a too-small change in the P_ψ period.

We next consider the opposite case, namely, the initial condition in 2012 October and model propagation forward in time to 2017 October. The results are shown in Figure 10. Obviously, here the red histograms (from the initial data in 2012 October) are more constrained than the blue histograms (resulting from rotation state vectors propagated using our model to 2017 October). The latter are more dispersed than the red histograms in Figure 9 because the less numerous and accurate observations in 2012 constrain the models with lower accuracy. Nevertheless, the principal features of the solution are still present: (i) the P_ϕ period changed adequately for the majority of cases, while (ii) the P_ψ period changed too little.

4.3.3. In Summary

So, while we are not able to provide exact proof that the change in P_ϕ and P_ψ periods between the 2012 and 2017 apparitions of 2012 TC4 is due to the YORP effect, we consider that the difference between the observations and model predictions can be accounted for by the model inaccuracy.

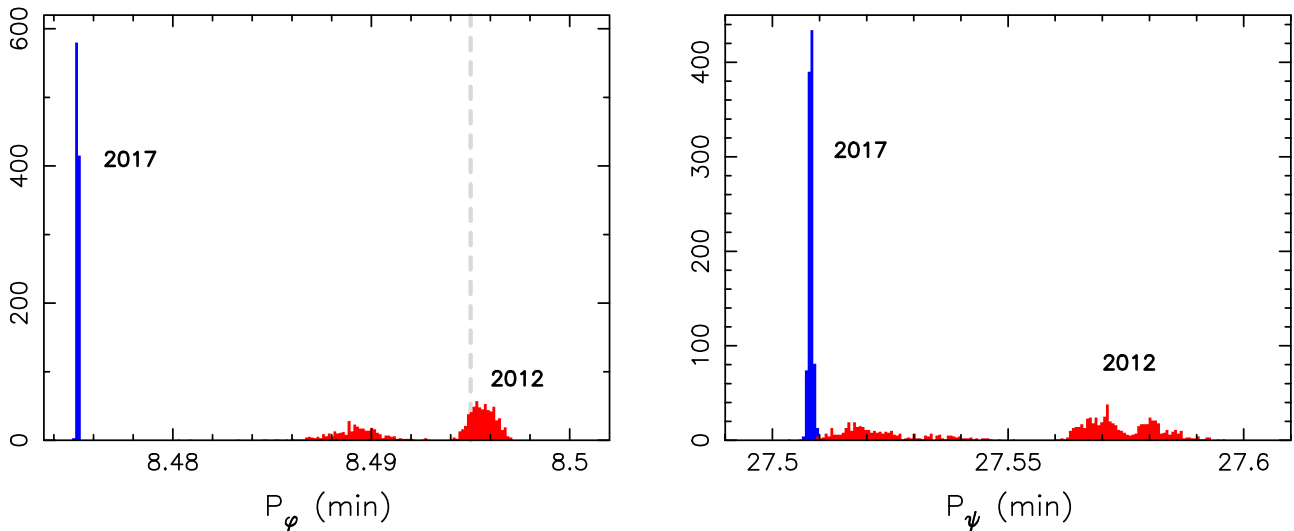


Figure 9. Same as Figure 8 but for nearly 1000 variant shape models of 2012 TC4 constructed from a combination of the 2012 and 2017 data. Data at the initial epoch MJD 58,032.19 (2017 October) are in blue. They have been propagated using our dynamical model to MJD 56,209.88 (2012 October), and the end states of these runs served to compute P_ϕ and P_ψ , shown by the red histograms.

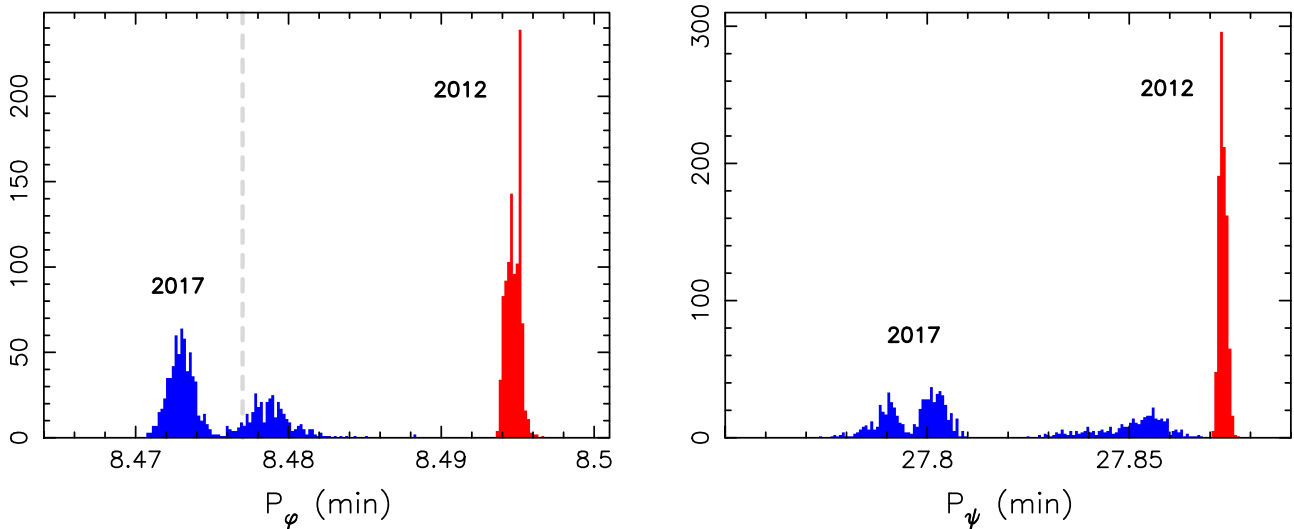


Figure 10. Same as Figure 9 (shape models constrained by both 2012 and 2017 observations), but now propagation was performed from the MJD 56,209.5 epoch in 2012 (red) to MJD 58,032.19 in 2017 (blue). The 2012 data constrain the rotation state solution less accurately and thus result in a larger scatter of the predicted periods P_ϕ and P_ψ in 2017. The vertical dashed line shows the mean value of the P_ϕ period from the 2017 October observations.

5. Discussion

In the previous section, we demonstrated that the observed change of the rotation state of 2012 TC4 between the two apparitions in 2012 and 2017 may possibly be explained as a result of the YORP effect. We also showed that the effect of the close encounter in 2012 October 12 on the rotation state was minimal, at least in a rigid-body approximation. However, since the YORP model—for the reasons explained—did not provide an exact match of the observations, and even left unresolved the issue of the observed energy change versus the model prediction, it is both useful and necessary to also briefly analyze possible alternative explanations. Here we discuss in some detail two plausible processes. We leave aside a third possibility, notably a mass loss from the surface of 2014 TC4 sometime in the period between the two observation campaigns (or during the 2012 Earth encounter). At first sight, this may look like an attractive explanation because the fast rotation of this body implies formally

negative gravitational attraction at the surface. Therefore, it takes only the effect of breaking cohesive bonds near the surface to make part of the body escape. This event would have an influence on rotational energy and angular momentum, both directly by the quanta carried away by escaping mass and by a change of TC4’s tensor of inertia. While possible, the caveats of this model are twofold: (i) first, the observational data do not have the resolution to provide conclusive information about a shape change of the body (which may not be large for the effect to work at the one-per-mile level), and, (ii) more importantly, in most scenarios, the process would lead to a decrease of the rotational angular momentum of TC4. Unlike in the two processes discussed below, we are not able to simply estimate the likelihood of this process.

5.1. Internal Energy Dissipation Effects

The individual solutions of 2012 TC4’s rotation parameters in 2012 and 2017 indicate that periods P_ψ and P_ϕ decreased in

the latter epoch (Figure 4). In terms of an osculating approximation with a free-top model, it implies that the wobbling motion of the angular momentum vector \mathbf{L} in the body-fixed frame moved toward the fundamental mode of its direction along the shortest axis of the inertia tensor. Note that the trajectory of \mathbf{L} in the body-fixed frame is uniquely parameterized with $p = 2BE/L^2$ (see, e.g., Appendix A and Landau & Lifshitz 1969). In quantitative terms, the change from the 2012 to 2017 state is expressed by $\delta p \simeq -6.2 \times 10^{-3}$ (Table 2). The average rate over a $\delta t \simeq 5$ yr interval would thus be $\delta p/\delta t \simeq -3.9 \times 10^{-11} \text{ s}^{-1}$.

In the YORP model presented above, the change in p was a composition of changes in both the energy E and angular momentum L . In fact, both E and L increased from 2012 to 2017 (Figure 7), but the composite effect was a decrease in p , in this case, $\delta p \simeq -4.6 \times 10^{-3}$, a similar value to that directly determined from osculating L and E above. Other processes may lead to approximately the same results by producing a different combination of energy and angular momentum changes. For instance, the effects of material inelasticity directly result in energy dissipation while preserving angular momentum. In this case, both E and p decrease with the direct relation $\delta E \simeq (L^2/2B)\delta p$.

In order to explore whether the observed effect of 2012 TC4's spin change could even be plausibly matched by internal energy dissipation, we used the model presented by Breiter et al. (2012). These authors assumed a fully triaxial geometry of the body but restricted their analysis of energy dissipation to the empirical description with a quality factor Q (see an alternative model of Frouard & Efroimsky 2017, where the authors described the energy dissipation using a Maxwell viscous liquid but allowed only a biaxial shape of the body). With these assumptions, they expressed the secular (i.e., wobbling cycle-averaged) rate of energy change in the following form:

$$\frac{\delta E}{\delta t} \simeq -\frac{a^4 \rho m \Omega^5}{\mu Q} \Psi, \quad (1)$$

where a is the semimajor axis of the body's triaxial approximation, ρ is its density, m is its mass, $\Omega = L/C$, and Ψ is a rather complicated factor depending on the nutation angle θ_{nut} (i.e., the tilt between \mathbf{L} and the shortest body axis; we find that θ_{nut} oscillates between $\simeq 16^\circ$ and $\simeq 46^\circ$, with a mean of $\simeq 30^\circ$), body axis ratios, and Lamé coefficients (see Breiter et al. 2012, Section 4.3). Finally, μ is the Lamé shear modulus (rigidity) and Q is the quality factor, empirically expressing the energy dissipation per wobbling cycle. The product μQ has been characteristic of studies involving energy dissipation in planetary science since the pioneering work of Burns & Safronov (1973; see, however, Prendergast 1958). While highly uncertain, the typical values of this parameter for asteroids range between 10^{11} and 5×10^{12} Pa (e.g., Harris 1994). Using $\delta E/\delta t \simeq (L^2/2B)\delta p/\delta t$ with the abovementioned $\delta p/\delta t$ value, we can now use Equation (1) to infer what values of μQ would be needed to explain the change in 2012 TC4's tumbling state in between the 2012 and 2017 close approaches. The remaining unknown parameter is Ψ , which we estimate to be $\simeq (1-5) \times 10^{-3}$. Plugging this value into Equation (1), we find μQ ranging from 4×10^5 to 4×10^6 Pa. Remarkably, such values are 4–5 orders of magnitude smaller than the usually adopted estimates. Therefore, unless the energy dissipation by internal friction is extraordinarily

high (and thus the μQ value is very small), this process cannot explain the observed rotation change of 2012 TC4. Note, additionally, that we considered the derivation of the needed μQ value within the energy dissipation model as a useful exercise to match the energy change. Such a model, however, would not explain the observed angular momentum change.

5.2. Impact by an Interplanetary Particle

Another alternative process to the radiation torques is that of an impact by an interplanetary meteoroid. However, in the following, we provide an argument that the likelihood of this happening at the level needed to explain the 2012 TC4 data is again very small. To that end, we used information from Bottke et al. (2020). They determined the meteoroid flux on a small asteroid, (101955) Bennu, using the state-of-the-art model MEM-3, allowing them to predict the parameters of meteoroids impacting a target body orbiting between Mercury and the asteroid belt (e.g., Moorhead et al. 2020). Note that the orbit of Bennu is similar to 2012 TC4, and we shall neglect the small flux differences that could result from a small orbital dissimilarity of these two objects (if anything, the flux would be slightly larger on Bennu because of its closer orbit to the Sun). In their Figure 2, Bottke et al. (2020) showed that 5 mg interplanetary particles, approximately 2 mm in size, strike Bennu with a frequency of $\simeq 60 \text{ yr}^{-1}$ with a median impact velocity of a little less than $\simeq 30 \text{ km s}^{-1}$. For 2012 TC4, we only need to rescale this number to account for a much smaller size; Bennu is an $\simeq 500$ m asteroid, while the characteristic size of 2012 TC4 is only $\simeq 10$ m. Therefore, the 5 mg flux on 2012 TC4 is about $\simeq 2.4 \times 10^{-2} \text{ yr}^{-1}$. The chances of being hit by such a particle in 5 yr is therefore merely $\simeq 0.12$. However, even if it had happened, the dynamical effect would be minimum. Estimating the change in rotational angular momentum L plainly by $\delta L/L \simeq (m/M)(v_{\text{imp}}/R\omega)$, where m and M are the masses of the particle and 2012 TC4, v_{imp} is the impact velocity, and R and ω are 2012 TC4's characteristic radius and rotational frequency, we would obtain $\delta L/L \simeq 2 \times 10^{-7}$. At least a 10,000 times larger effect would be needed to approach the level observed for 2012 TC4, and this would require an impacting particle at least 20 times larger, i.e., 5 cm or more. Because MEM-3 incorporates the flux dependence on mass from Grün et al. (1985), thus $\propto m^{-4/3}$, the chances that 2012 TC4 was hit by a 5 cm meteoroid between 2012 and 2017 is only $\simeq 6 \times 10^{-7}$. We thus conclude that the chances that the observed effect was produced by an impact of an interplanetary particle are negligibly small and may be discarded.

6. Conclusions

The photometric data of 2012 TC4 collected during its two close approaches to Earth in 2012 and 2017 clearly show that this asteroid is in an excited rotation state. Fourier analysis of the 2012 and 2017 data sets finds two unique periods in the signal, and these two periods are significantly different, which means that the rotation state of TC4 must have changed slowly between 2012 and 2017 or suddenly during the 2012 flyby (the 2017 flyby was after the photometric observations). This detection of period change is robust and not model-dependent.

The periods detected by Fourier analysis were used to constrain the physical rotation and precession periods of the tumbling rotation state. We found only one physically acceptable solution that fits the photometric data, namely, the free-tumbling situation about the shortest axis of the inertia tensor (SAM mode). When modeling light-curve sets from 2012 and 2017 separately, the

shape models are similar, with about the same direction of the angular momentum vector, but the rotation and precession periods are significantly different, and there is no combination of parameters that would provide an acceptable fit to the whole data set. The change of the physical periods of tumbling is consistent with the change revealed by Fourier analysis. Including this period change in our model, we were able to fit all available photometry from both apparitions. The difference in periods for the 2012 and 2017 apparitions is much larger than any possible random or model error, so this model-based detection of period change is significant and robust.

Having detected the period change and created a physical model of TC4, we looked for a possible explanation for this change. First, we show that the effect of the close encounter in 2012 on the rotation state was negligibly small compared to the detected change of the rotation state. Second, we show that a plausible explanation is the YORP effect; the numerical simulation of the rotation dynamics based on our shape model of TC4 gives a general agreement with the observed period change. Although the match is not ideal, we believe that the discrepancy is caused by simplification in our YORP model and uncertainties in the shape model and other parameters. We also show that the other two possible mechanisms that could affect the rotation state—namely, the internal energy dissipation and impacts of interplanetary particles—are too small to cause the measured effect, so YORP remains the only plausible explanation of the observed change of the rotation state of 2012 TC4. Accepting this explanation, this is the first detection of YORP acting on a tumbling asteroid.

This research is supported by the Korea Astronomy and Space Science Institute (KASI). The work at Charles University and Ondřejov Observatory was supported by the Czech Science

The kinematical part of the problem describes the orientation of the asteroid in the inertial frame. For simplicity, we assume the asteroid is a rigid body, allowing us to unambiguously define a proper body-fixed frame. The easiest choice has (i) an origin in the asteroid's center of mass and (ii) axes coinciding with the principal axes of the inertia tensor \mathbf{I} (therefore, $\mathbf{I} = \text{diag}(A, B, C)$, with $A \leq B \leq C$). The transformation between the inertial and body-fixed frames is conventionally parameterized by a set of Euler angles, most often the 3–1–3 sequence of the precession angle ϕ , nutation angle θ , and angle of proper rotation ψ . However, instead of the three Euler angles (ϕ, θ, ψ) , here we use the Rodrigues–Hamilton parameters $\boldsymbol{\lambda} = (\lambda_0, \lambda_1, \lambda_2, \lambda_3)$ (e.g., Whittaker 1917). Their relation to the Euler angles is given by (i) $\lambda_0 + \iota\lambda_3 = \cos \frac{\theta}{2} \exp \left[\frac{\iota}{2}(\psi + \phi) \right]$ and (ii) $\lambda_2 + \iota\lambda_1 = \iota \sin \frac{\theta}{2} \exp \left[\frac{\iota}{2}(\psi - \phi) \right]$ (ι is a complex unit). One can easily verify a constraint: $\lambda_0^2 + \lambda_1^2 + \lambda_2^2 + \lambda_3^2 = 1$ (in our numerical runs, satisfied with $\leq 10^{-13}$ accuracy). The sacrifice of using four instead of three parameters pays off with at least two advantages. First, the parameterization by Euler angles is unstable when in or near the $\sin \theta = 0$ state. No such problem occurs when using the Rodrigues–Hamilton parameters, which provide a uniformly nonsingular description of the rotation. Second, Euler-angle parameterization necessarily requires the use of trigonometric functions. Instead, manipulation with the Rodrigues–Hamilton parameters is limited to simple algebraic functions, in fact, quadratic at maximum, as shown below in Equations (A1) and (A2). For that reason, the use of the four Rodrigues–Hamilton parameters does not even slow down the computations in a noticeable way.

The rotation matrix \mathbf{A} needed for the vector transformation from the inertial frame to the body-fixed frame is a simple quadratic form of $\boldsymbol{\lambda}$, namely,

$$\mathbf{A} = \begin{pmatrix} \lambda_0^2 + \lambda_1^2 - \lambda_2^2 - \lambda_3^2 & , & 2(\lambda_0\lambda_3 + \lambda_1\lambda_2) & , & 2(\lambda_1\lambda_3 - \lambda_0\lambda_2) \\ 2(\lambda_1\lambda_2 - \lambda_0\lambda_3) & , & \lambda_0^2 + \lambda_2^2 - \lambda_1^2 - \lambda_3^2 & , & 2(\lambda_0\lambda_1 + \lambda_2\lambda_3) \\ 2(\lambda_0\lambda_2 + \lambda_1\lambda_3) & , & 2(\lambda_2\lambda_3 - \lambda_0\lambda_1) & , & \lambda_0^2 + \lambda_3^2 - \lambda_1^2 - \lambda_2^2 \end{pmatrix}. \quad (\text{A1})$$

Foundation (grant 20-04431S). The work by C.-H.K. was supported by the Basic Science Research Program through the National Research Foundation of Korea funded by the Ministry of Education (2018R1D1A1A09081827, 2020R1A4A2002885). This research has made use of the KMTNet system operated by the Korea Astronomy and Space Science Institute (KASI), and the data were obtained at SAAO in South Africa. We appreciate all astronomers who uploaded or shared their previously published light curves of 2012 TC4 used in this paper.

Appendix A Rotational Dynamics of 2012 TC4

In this appendix, we summarize the variables and mathematical approach used for propagation of the 2012 TC4 rotation state between the 2012 and 2017 epochs (Section 4). This is obviously a classical piece of mechanics that can be found in many textbooks (e.g., Landau & Lifshitz 1969; Goldstein 1980). For that reason, we keep our description to a very minimum.

The inverse transformation is represented by a transposed matrix \mathbf{A}^T . The asteroid's rotation is represented with the angular velocity vector $\boldsymbol{\omega}$, whose components in the body-fixed frame are $(\omega_1, \omega_2, \omega_3)$. Their relation to the time derivatives of the Rodrigues–Hamilton parameters is simply

$$\frac{d\boldsymbol{\lambda}}{dt} = \frac{1}{2} \mathbf{P} \cdot \boldsymbol{\lambda}, \quad (\text{A2})$$

where

$$\mathbf{P} = \begin{pmatrix} 0 & , & -\omega_1 & , & -\omega_2 & , & -\omega_3 \\ \omega_1 & , & 0 & , & \omega_3 & , & -\omega_2 \\ \omega_2 & , & -\omega_3 & , & 0 & , & \omega_1 \\ \omega_3 & , & \omega_2 & , & -\omega_1 & , & 0 \end{pmatrix}. \quad (\text{A3})$$

This explicitly linear differential equation for $\boldsymbol{\lambda}$ cannot be solved in a trivial way because $\mathbf{P} = \mathbf{P}(\boldsymbol{\omega})$, and the angular momentum vector is a time-dependent variable. The anti-symmetry of \mathbf{P} implies conservation of the abovementioned quadratic constraint of $\boldsymbol{\lambda}$.

The dynamical part of the problem expresses Newton's principle that a change of the rotational (intrinsic) angular momentum $\mathbf{L} = \mathbf{I} \cdot \boldsymbol{\omega}$ is given by the applied torque \mathbf{M} . The tradition is to state this rule in the body-fixed frame, where \mathbf{I} is constant and even diagonal in our choice of axes, such that

$$\frac{d\mathbf{L}}{dt} + \boldsymbol{\omega} \times \mathbf{L} = \mathbf{M}. \quad (\text{A4})$$

Equations (A2) and (A4) define the problem of the asteroid's rotation in our set of seven parameters $(\boldsymbol{\lambda}, \boldsymbol{\omega})$. Once the torques \mathbf{M} are specified, we numerically integrate this system of differential equations with the initial data determined from the set of observations (either forward in time, if the 2012 data are used, or backward in time, if the 2017 data are used). We use the Burlish–Stoer integration scheme with tightly controlled accuracy. We also note another useful quantity, namely, the energy of rotational motion about the center given by $E = \frac{1}{2} \boldsymbol{\omega} \cdot \mathbf{L}$. In the classical problem of a free top (i.e., $\mathbf{M} = \mathbf{0}$), both E and \mathbf{L} in the inertial frame are conserved. In the body-fixed frame, only $L = |\mathbf{L}|$ is constant. Nevertheless, conservation of E and L (together with the principal values of the inertia tensor A , B , and C) uniquely determines the wobbling trajectory of \mathbf{L} in the body-fixed frame (e.g., Landau & Lifshitz 1969; Deprit & Elipe 1993). There are two options for this motion: (i) SAM, when \mathbf{L} circulates about the $+z$ or $-z$ body axis, or (ii) LAM, when \mathbf{L} circulates about the $+x$ or $-x$ body axis. A useful discriminator of the two is yet another conserved and nondimensional quantity in the free-top problem, namely, $p = 2BE/L^2$: (i) SAM is characterized by p values in between $\beta = B/C$ and 1, while (ii) LAM is characterized by p values in between 1 and $\alpha = B/A$. Note that $\Delta = B/p$ plays an important role in the description of the free-top problem using Hamiltonian tools (e.g., Deprit & Elipe 1993; Breiter et al. 2011). The free-top motion of \mathbf{L} in the body-fixed frame is easily integrable using Jacobi elliptic functions. When plugged into the kinematical Equation (A3), one can also obtain a solution for $\boldsymbol{\lambda}$ or the Euler angles (ϕ, θ, ψ) (e.g., Landau & Lifshitz 1969). Those of ψ and θ are strictly periodic with a period of (SAM relevant for 2012 TC4 assumed here)

$$P_\psi = \frac{C}{L} \frac{4\beta K(k)}{\sqrt{(1-\beta)(\beta/\alpha-p)}}, \quad (\text{A5})$$

where $K(k)$ is a complete elliptic integral of the first kind, with the modulus k given by

$$k^2 = \frac{(\beta/\alpha - 1)(p - \beta)}{(1 - \beta)(\beta/\alpha - p)} \quad (\text{A6})$$

(the motion of θ has a periodicity of $P_\psi/2$). The motion of the precession angle ϕ is not periodic. Nevertheless, a fully analytical solution still exists and is composed of two parts, the first of which has periodicity P_ψ , and the second has another periodicity, generally incommensurable with P_ψ (e.g., Landau & Lifshitz 1969). Yet it is both practical and conventional to define an approximate periodicity P_ϕ of ϕ . We use the definition of Kaasalainen (2001, Equation (A.11)), namely, numerically determining an advance in the ϕ angle over the P_ψ period (this, in principle, averages out the contribution of the P_ψ periodic part in the ϕ solution). When weak torques are

applied, the free-top solution still represents a very useful (osculating) template with all above-discussed variables, such as E , L , p , P_ψ , or P_ϕ , adiabatically changing in time.

Finally, we discuss the torques used in our analysis. The first class is due to the gravitational tidal fields of the Sun and Earth. Assume a point-mass source M specified in the body-fixed frame of the asteroid with a position vector \mathbf{R} . Using the quadrupole part of the exterior perturber tidal field, we have (e.g., Fitzpatrick 1970; Takahashi et al. 2013)

$$\mathbf{M}_{\text{grav}} = \frac{3GM}{R^5} \mathbf{R} \times (\mathbf{I} \cdot \mathbf{R}). \quad (\text{A7})$$

We neglect the formally dipole part of the tidal field, which could only occur if the true center of mass of the asteroid is slightly displaced from the assumed location (determined by using the assumption of homogeneous density; see, e.g., Takahashi et al. 2013). Note that the position of all bodies, the asteroid, the Sun, and the Earth, are primarily determined using the numerical integration of the orbital problem in the inertial frame (or, actually, the displaced heliocentric frame). In our case, we numerically integrated planetary orbits, including Earth, and 2012 TC4 in the heliocentric system by taking the initial data from the NEODYs website (<https://newton.spacedys.com/neody/>). We output the necessary positions every 170 s, enough for the purpose of the 2012 TC4's rotation dynamics. We also compared our solution with that available at the JPL Horizons system (<http://ssd.jpl.nasa.gov/?horizons>) and found a very good correspondence with tiny differences, not meaningful for our application. The relative position \mathbf{R} in Equation (A7) is determined by (i) the difference of the corresponding bodies in our orbital solution and (ii) transformation to the body-fixed frame. As a result, $\mathbf{M}_{\text{grav}} = \mathbf{M}_{\text{grav}}(t, \boldsymbol{\lambda})$. The steep dependence $M_{\text{grav}} \propto R^{-3}$ implies that the Earth effect is nonnegligible only during the close encounters with this planet (e.g., Figure 5).

Our analysis also includes the radiation torque known as the YORP effect (e.g., Bottke et al. 2006; Vokrouhlický et al. 2015a). Because of the tumbling rotation state of 2012 TC4, we resort to the simplest variant, namely, a limit of zero thermal inertia (the effects of finite thermal inertia were studied only for objects rotating about the shortest axis of the inertia tensor so far; e.g., Čapek & Vokrouhlický 2004; Golubov & Krugly 2012). In this approximation, the radiation torque is given by (e.g., Rubincam 2000; Vokrouhlický & Čapek 2002)

$$\mathbf{M}_{\text{YORP}} = -\frac{2F}{3c} \int H[\mathbf{n} \cdot \mathbf{n}_0] (\mathbf{n} \cdot \mathbf{n}_0) \mathbf{r} \times d\mathbf{S}, \quad (\text{A8})$$

where F is the solar radiation flux at the location of the asteroid, and c is the light velocity. The integral in Equation (A8) is performed over the surface of the body characterized by an ensemble of outward-oriented surface elements $d\mathbf{S} = \mathbf{n} dS$, where \mathbf{n} is the normal to the surface, and \mathbf{r} is the position of the surface element with respect to the origin of the body-fixed frame. The unit vector of the solar position in the body-fixed frame is denoted with \mathbf{n}_0 , and $H[x]$ is the Heaviside step function (its presence in the integrand of Equation (A8) implies that a nonzero contribution to the radiation torque is provided by surface units for which the Sun is above local horizon). In fact, our code includes an even more complex feature of self-

shadowing of surface units, but this is not active in the case of 2012 TC4, whose resolved shape is convex. The factor $2/3$ on the right-hand side of Equation (A8) is due to the assumption of Lambertian reradiation from the surface. More complicated assumptions about the directionality of the thermally emitted radiation from the surface, such as the beaming effects (e.g., Rozitis & Green 2012), are presently not implemented in the code. The light-curve inversion obviously allows only a finite accuracy in the shape determination of the body, typically a convex polyhedron with little more than 1000 surface facets. It is already known that this fact is an obstacle to an accurate evaluation of the YORP torque, which may sensitively depend on smaller-scale surface irregularities not resolved by our shape model. The formal integration in Equation (A8) is therefore represented with a summation over the surface units of the

resolved shape model. We use algebra from Dobrovolskis (1996) to determine all necessary variables. This also means we assume a constant density distribution in the body.

Appendix B Light-curve Fits

Here we show how the model fits the data. In all plots below (Figures B1–B7), blue dots are individual photometric measurements, and the red light curve is what the best-fit model from Section 3.3 predicts. The relative brightness on the vertical axis is scaled to have a mean value of 1. The ticks on the horizontal axis are 10 minutes apart, and the scale is the same for all plots. More information about light curves can be found in Table 1.

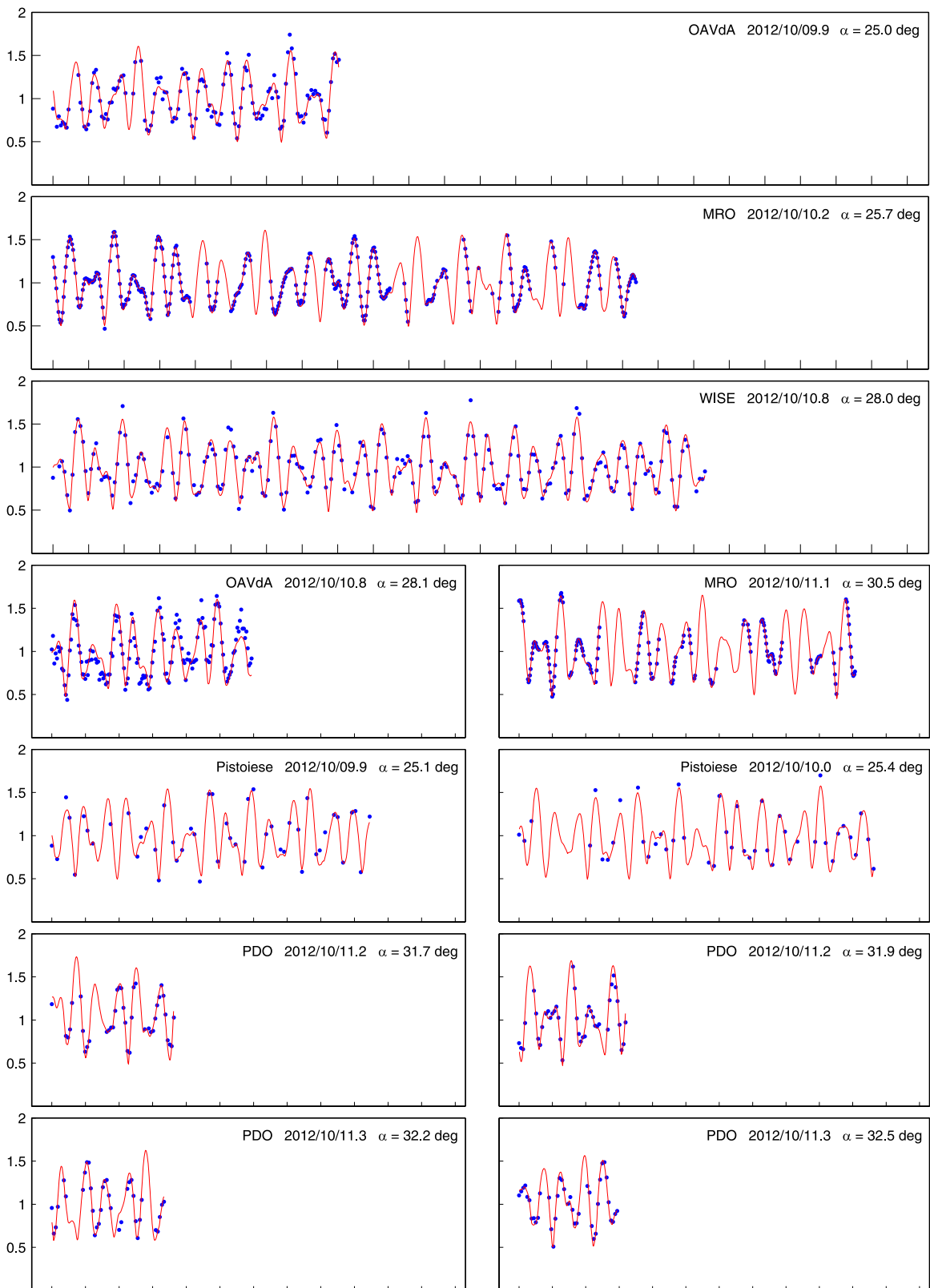


Figure B1. Light-curve fits for data in 2012. The photometric light-curve data shown in this figure are available as “data behind the figure.” (The data used to create this figure are available.)

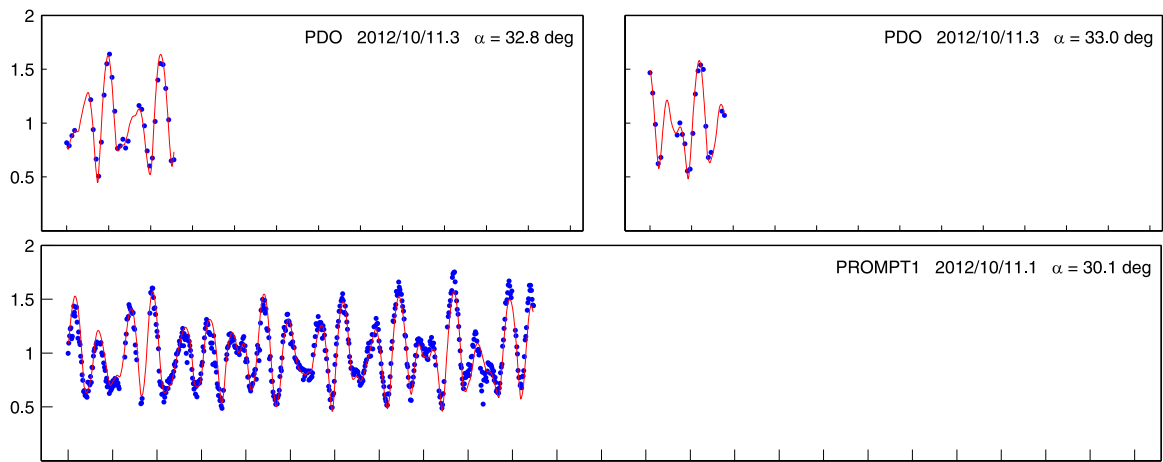


Figure B2. Light-curve fits for data in 2012. The photometric light-curve data shown in this figure are available as “data behind the figure.” (The data used to create this figure are available.)

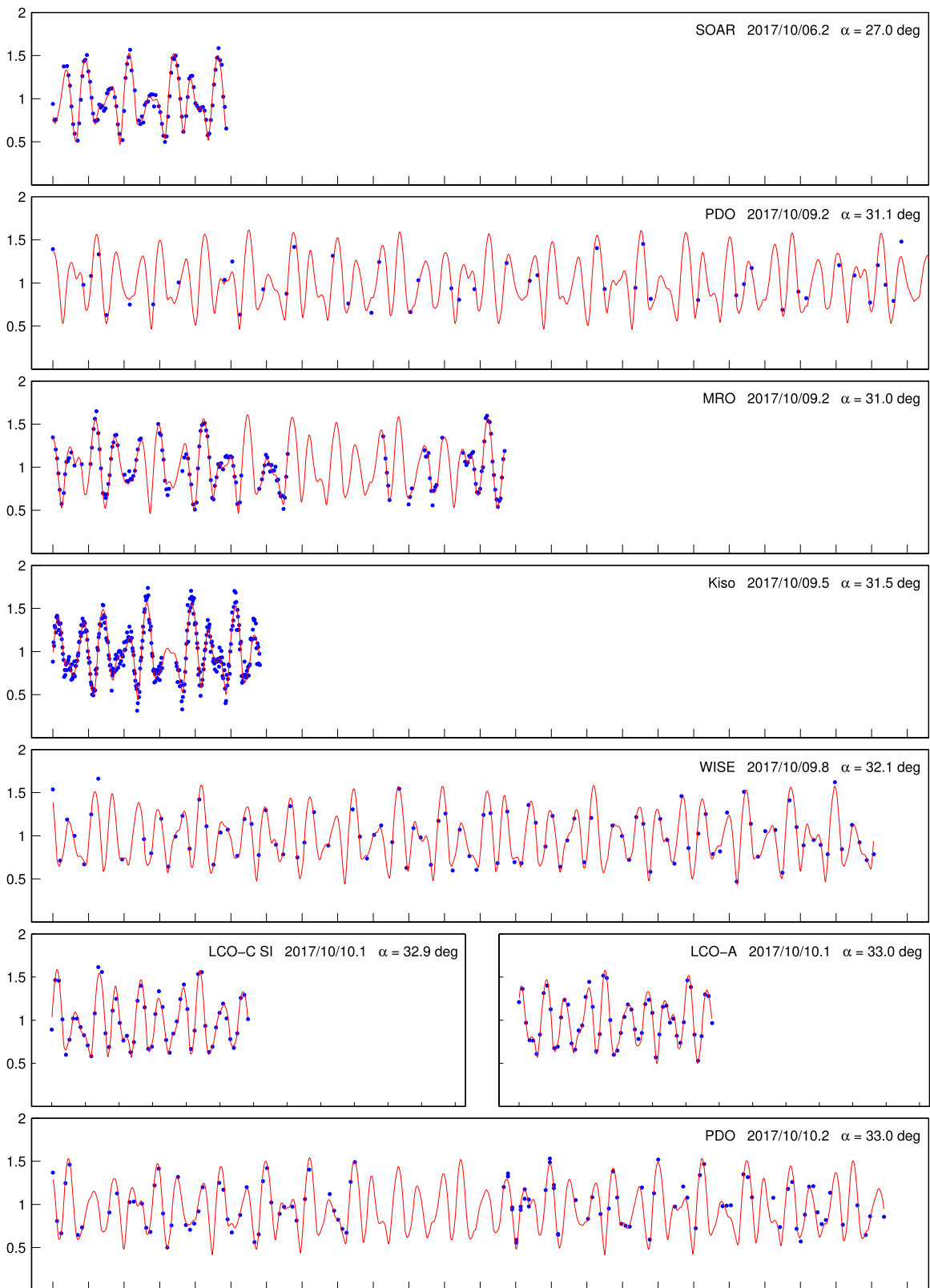


Figure B3. Light-curve fits for data in 2017. The photometric light-curve data shown in this figure are available as “data behind the figure.” (The data used to create this figure are available.)

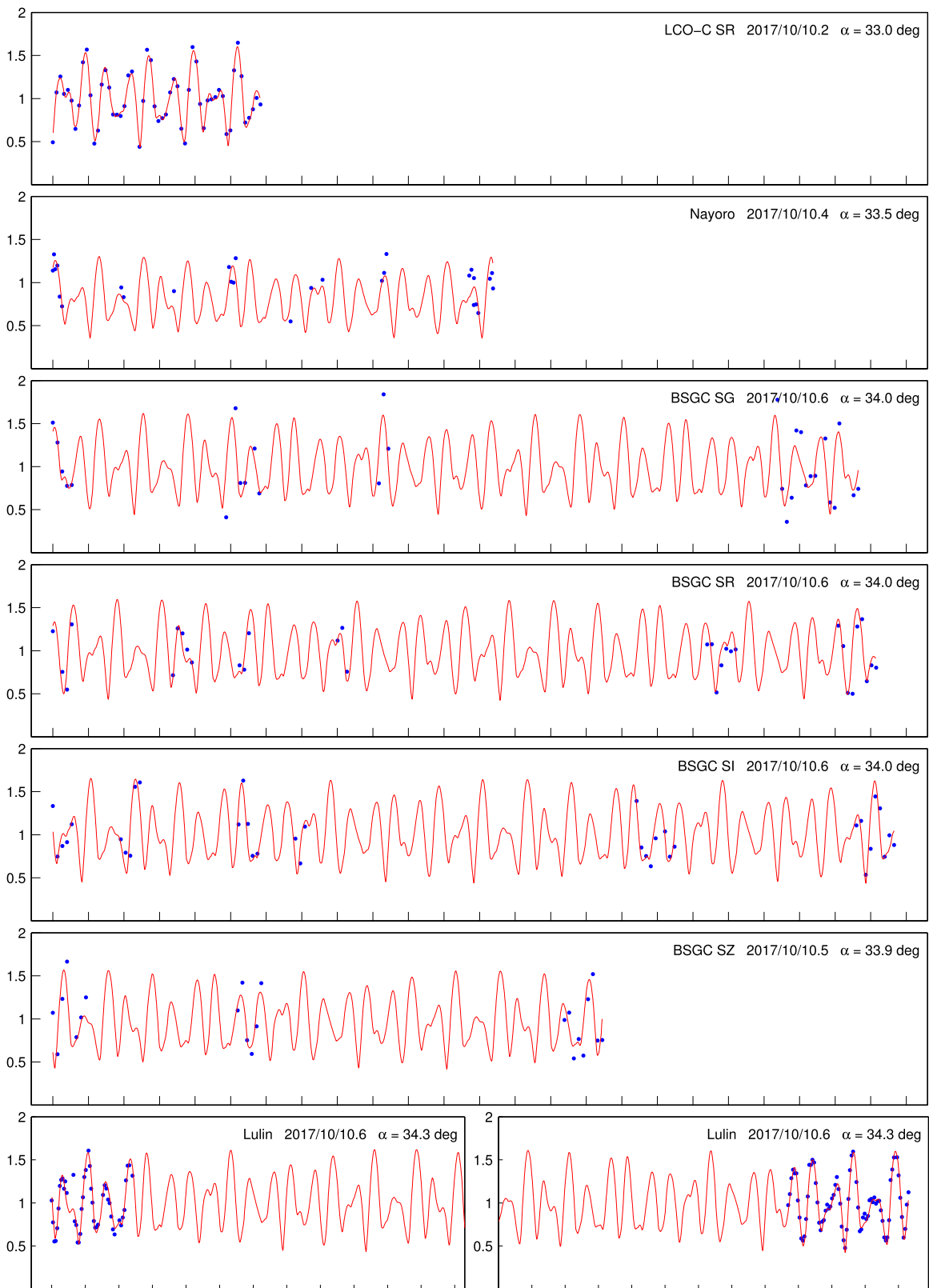


Figure B4. Light-curve fits for data in 2017. The photometric light-curve data shown in this figure are available as “data behind the figure.” (The data used to create this figure are available.)

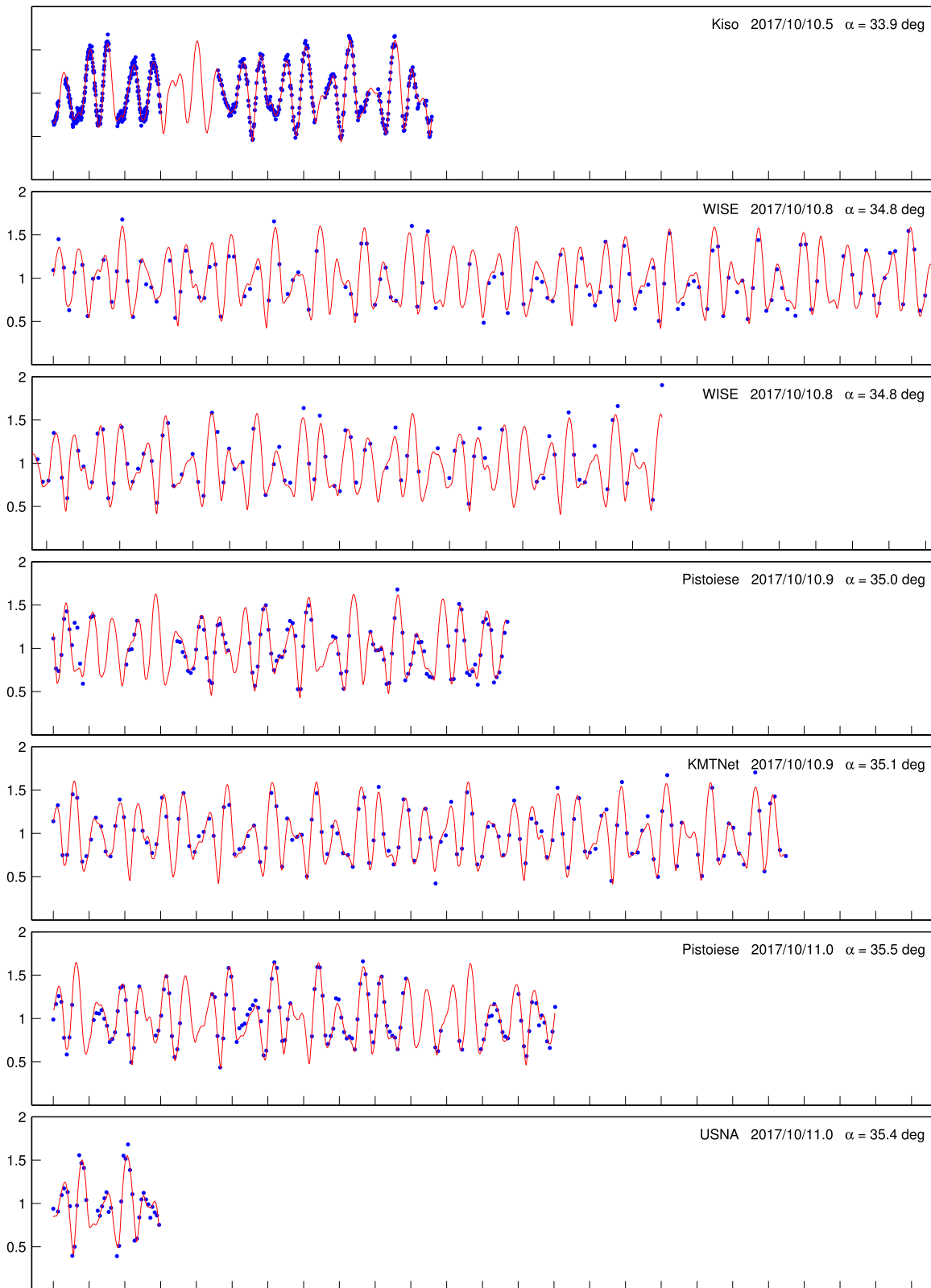


Figure B5. Light-curve fits for data in 2017. The photometric light-curve data shown in this figure are available as “data behind the figure.” (The data used to create this figure are available.)

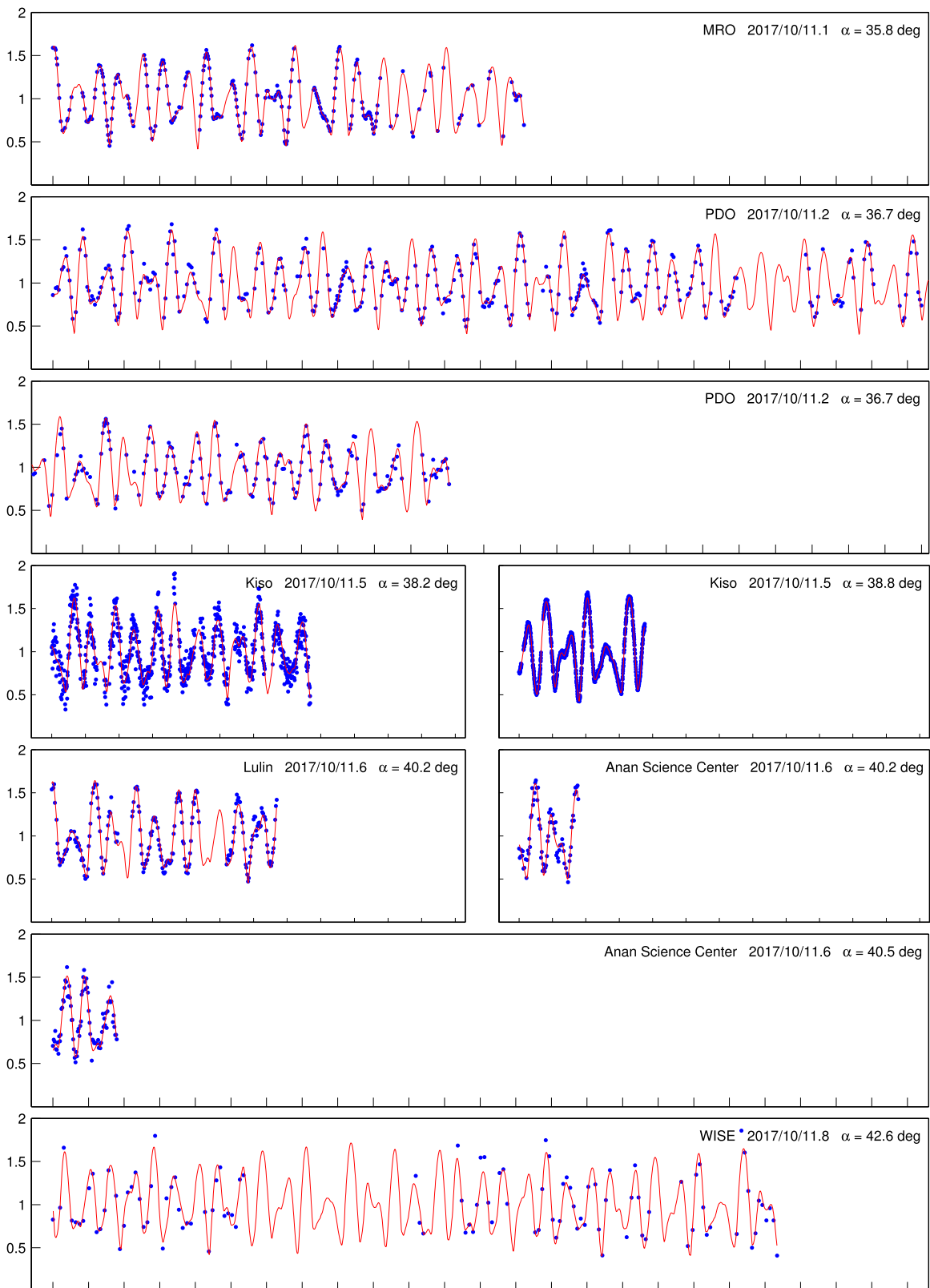


Figure B6. Light-curve fits for data in 2017. The photometric light-curve data shown in this figure are available as “data behind the figure.” (The data used to create this figure are available.)

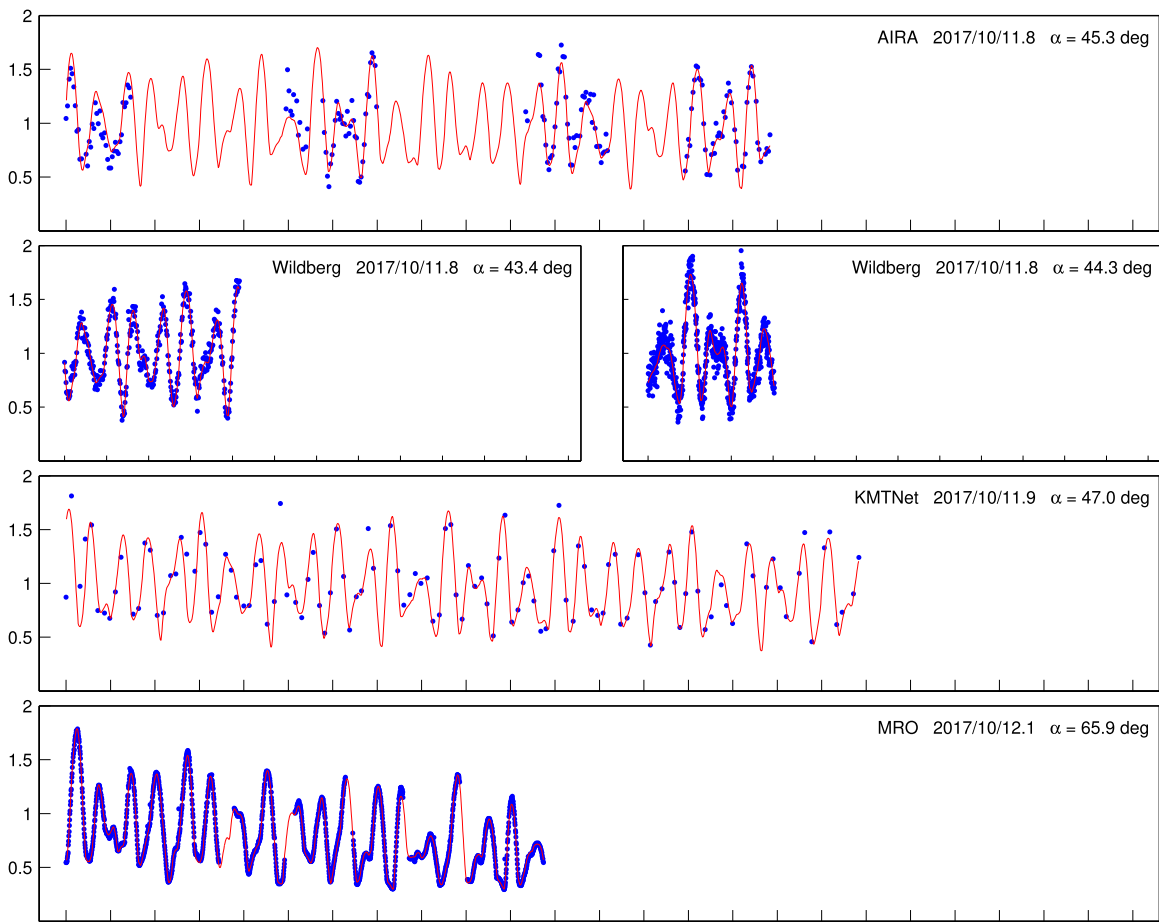


Figure B7. Light-curve fits for data in 2017. The photometric light-curve data shown in this figure are available as “data behind the figure.” (The data used to create this figure are available.)

ORCID iDs

Hee-Jae Lee <https://orcid.org/0000-0002-6839-075X>
 Josef Ďurech <https://orcid.org/0000-0003-4914-3646>
 David Vokrouhlický <https://orcid.org/0000-0002-6034-5452>
 Chun-Hwey Kim <https://orcid.org/0000-0001-8591-4562>

References

- Bottke, W. F., Moorhead, A., Connolly, H. C., et al. 2020, *JGR*, **125**, e06282
 Bottke, W. F., Vokrouhlický, D., Rubincam, D. P., & Nesvorný, D. 2006, *AREPS*, **34**, 157
 Breiter, S., Rožek, A., & Vokrouhlický, D. 2011, *MNRAS*, **417**, 2478
 Breiter, S., Rožek, A., & Vokrouhlický, D. 2012, *MNRAS*, **427**, 755
 Burns, J. A., & Safronov, V. S. 1973, *MNRAS*, **165**, 403
 Čapek, D., & Vokrouhlický, D. 2004, *Icar*, **172**, 526
 Carbognani, A. 2014, *MPBu*, **41**, 4
 Cicalò, S., & Scheeres, D. J. 2010, *CeMDA*, **106**, 301
 Delbó, M., Mueller, M., Emery, J. P., Rozitis, B., & Capria, M. T. 2015, in *Asteroids IV*, ed. P. Michel, F. E. DeMeo, & W. F. Bottke (Tucson, AZ: Univ. Arizona Press), 107
 Deprit, A., & Elipe, A. 1993, *JAnSc*, **41**, 603
 Dobrovolskis, A. R. 1996, *Icar*, **124**, 698
 Ďurech, J., Sidorin, V., & Kaasalainen, M. 2010, *A&A*, **513**, A46
 Farnocchia, D., Chesley, S. R., Vokrouhlický, D., et al. 2013, *Icar*, **224**, 1
 Fitzpatrick, P. 1970, *Principles of Celestial Mechanics* (New York: Academic)
 Frouard, J., & Efroimsky, M. 2017, *CeMDA*, **129**, 177
 Goldstein, H. 1980, *Classical Mechanics* (Reading, MA: Addison-Wesley)
 Golubov, O., & Krugly, Y. N. 2012, *ApJL*, **752**, L11
 Grün, E., Zook, H. A., Fechtig, H., & Giese, R. H. 1985, *Icar*, **62**, 244
 Hapke, B. 1993, *Theory of Reflectance and Emittance Spectroscopy* (Cambridge: Cambridge Univ. Press)
 Harris, A. W. 1994, *Icar*, **107**, 209
 Kaasalainen, M. 2001, *A&A*, **376**, 302
 Kaasalainen, M., & Torppa, J. 2001, *Icar*, **153**, 24
 Kim, S.-L., Lee, C.-U., Park, B.-G., et al. 2016, *JKAS*, **49**, 37
 Landau, L., & Lifshitz, E. 1969, *Mechanics* (Oxford: Pergamon)
 Lee, H. J., Ďurech, J., Kim, M. J., et al. 2020, *A&A*, **635**, A137
 Lin, Z.-Y., Ip, W.-H., & Ngeow, C.-C. 2019, *P&SS*, **166**, 54
 Lowry, S. C., Fitzsimmons, A., Pravec, P., et al. 2007, *Sci*, **316**, 272
 Marsden, B. G., Sekanina, Z., & Yeomans, D. K. 1973, *AJ*, **78**, 211
 Mommert, M., Hora, J. L., Farnocchia, D., et al. 2014, *ApJ*, **786**, 148
 Moorhead, A. V., Kingery, A., & Ehlert, S. 2020, *JSpRo*, **57**, 160
 Odden, C. E., Verhaegh, J. C., McCullough, D. G., & Briggs, J. W. 2013, *MPBu*, **40**, 176
 Polishook, D. 2013, *MPBu*, **40**, 42
 Pravec, P., Harris, A. W., Scheirich, P., et al. 2005, *Icar*, **173**, 108
 Pravec, P., Scheirich, P., Ďurech, J., et al. 2014, *Icar*, **233**, 48
 Pravec, P., Šarounová, L., & Wolf, M. 1996, *Icar*, **124**, 471
 Prendergast, K. H. 1958, *AJ*, **63**, 412
 Raab, H. 2012, *Astrometrica: Astrometric Data Reduction of CCD Images*, ver. 4.10.2.433, Astrophysics Source Code Library, ascl:1203.012
 Reddy, V., Kelley, M. S., Farnocchia, D., et al. 2019, *Icar*, **326**, 133
 Roeser, S., Demleitner, M., & Schilbach, E. 2010, *AJ*, **139**, 2440
 Rozitis, B., & Green, S. F. 2012, *MNRAS*, **423**, 367
 Rubincam, D. P. 2000, *Icar*, **148**, 2
 Ryan, W., & Ryan, E. V. 2017, *AAS/DPS Meeting*, **49**, 204.06
 Scheirich, P., Ďurech, J., Pravec, P., et al. 2010, *M&PS*, **45**, 1804
 Sonka, A. B., Gomea, A. I., Anghel, S., & Birlan, M. 2017, *RoAJ*, **27**, 223
 Spjuth, S., Jorda, L., Lamy, P. L., Keller, H. U., & Li, J.-Y. 2012, *Icar*, **221**, 1101

- Takahashi, Y., Busch, M. W., & Scheeres, D. J. 2013, *AJ*, 146, 95
- Urakawa, S., Ohsawa, R., Sako, S., et al. 2019, *AJ*, 157, 155
- Vokrouhlický, D. 1998, *A&A*, 335, 1093
- Vokrouhlický, D., Bottke, W. F., Chesley, S. R., Scheeres, D. J., & Statler, T. S. 2015a, in *Asteroids IV*, ed. P. Michel, F. E. DeMeo, & W. F. Bottke (Tucson, AZ: Univ. Arizona Press), 509
- Vokrouhlický, D., Breiter, S., Nesvorný, D., & Bottke, W. F. 2007, *Icar*, 191, 636
- Vokrouhlický, D., Farnocchia, D., Čapek, D., et al. 2015b, *Icar*, 252, 277
- Vokrouhlický, D., Pravec, P., Ďurech, J., et al. 2017, *AJ*, 153, 270
- Vokrouhlický, D., & Čapek, D. 2002, *Icar*, 159, 449
- Vokrouhlický, D., Čapek, D., Chesley, S. R., & Ostro, S. J. 2005, *Icar*, 173, 166
- Warner, B. D. 2006, *A Practical Guide to Lightcurve Photometry and Analysis* (Berlin: Springer)
- Warner, B. D. 2013, *MPBu*, 40, 71
- Warner, B. D. 2018, *MPBu*, 45, 19
- Warner, B. D., Stephens, R. D., & Harris, A. W. 2011, *MPBu*, 38, 172
- Whittaker, E. 1917, *A Treatise on the Analytical Dynamics of Particles and Rigid Bodies* (Cambridge: Cambridge Univ. Press)